nature communications

Article

https://doi.org/10.1038/s41467-024-55294-8

The FvABF3-FvALKBH10B-FvSEP3 cascade regulates fruit ripening in strawberry

Received: 15 February 2024

Accepted: 6 December 2024

Published online: 30 December 2024

Check for updates

Renkun Tang[1,2,3], Xiaoyu Duan[1,2,3], Leilei Zhou[1,2], Guangtong Gao[1,2,3], Jinying Liu[1,2,3], Yuying Wang[1,2], Xingfeng Shao[4] & Guozheng Qin[1,2,3]

Fruit ripening is a highly-orchestrated process that requires the fine-tuning and precise control of gene expression, which is mainly governed by phytohormones, epigenetic modifiers, and transcription factors. How these intrinsic regulators coordinately modulate the ripening remains elusive. Here we report the identification and characterization of FvALKBH10B as an N^6-methyladenosine (m^6A) RNA demethylase necessary for the normal ripening of strawberry (*Fragaria vesca*) fruit. *FvALKBH10B* is induced by phytohormone abscisic acid (ABA), and ABA-Responsive Element Binding Factor 3 (FvABF3), a master regulator in ABA signaling, is responsible for this activation. *FvALKBH10B* mutation leads to a delay in fruit ripening and causes global m^6A hypermethylation of 1859 genes. Further analyses show that FvALKBH10B positively modulates the mRNA stability of *SEPALLATA3* (*FvSEP3*) encoding a transcription factor via m^6A demethylation. In turn, FvSEP3 targets numerous ripening-related genes including those associated with biosynthesis of ABA and anthocyanin and regulates their expression. Our findings uncover an FvABF3-FvALKBH10B-FvSEP3 cascade in controlling fruit ripening in strawberry and provide insights into the complex regulatory networks involved in this process.

Ripening is the final stage of fruit development that involves a series of physiological and biochemical changes in the color, flavor, aroma, and texture[1]. Due to the specificity of this developmental process to plant biology and its pivotal impact on fruit nutritional quality and shelf life, the ripening of fruit has attracted considerable attention. Fruit ripening is regulated by both external environmental cues and intrinsic developmental signals[2]. Plant hormone ethylene plays a key role in controlling the ripening of a group of fleshy fruits called climacteric fruits, e.g. tomato, apple, and banana, and substantial insights have been made toward the mechanisms of ethylene-induced fruit ripening[2,3]. In contrast, the ripening of another group of fleshy fruits, namely non-climacteric fruits, e.g. strawberry, grape, and citrus, appears to be ethylene-independent. Instead, abscisic acid (ABA) is responsible for the ripening of non-climacteric fruit[4,5], although the molecular basis of how ABA regulates fruit ripening is poorly understood.

As one of the most important phytohormones known, ABA is synthesized via the mevalonate pathway using C40 carotenoid precursors[6]. In this process, 9-*cis*-epoxycarotenoid dioxygenase (NCED) serves as the rate-limiting enzyme[6]. The ABA core signaling pathway comprises three protein classes: Pyrabactin Resistance/Pyrabactin Resistance-like/Regulatory Component of ABA Receptor (PYR/PYL/RCAR), the ABA receptors; Protein Phosphatase 2 C (PP2C) group A family, the negative regulators; SNF1-Related Protein Kinases type 2 (SnRK2s), the positive regulators[7]. In the absence of ABA, the ABA receptors are inactivated and the PP2C proteins inhibit the SnRK2 proteins. Upon ABA binding, the PYR/PYL/RCAR receptors inhibit PP2C activity, allowing the activation of SnRK2s through autophosphorylation. Activated SnRK2s then phosphorylate their downstream key transcriptional regulators, such as the ABA-Responsive Element Binding Factors/Proteins (ABFs/AREBs) transcription factors, which

[1]State Key Laboratory of Plant Diversity and Specialty Crops, Institute of Botany, Chinese Academy of Sciences, Beijing 100093, China. [2]China National Botanical Garden, Beijing 100093, China. [3]University of Chinese Academy of Sciences, Beijing 100049, China. [4]College of Food Science and Engineering, Ningbo University, Ningbo 315800, China. e-mail: gzqin@ibcas.ac.cn

bind to the ABA-responsive element (ABRE) in the promoters of ABA-inducible genes and modulate their expression[7]. Recently, it was shown that repression of ABA biosynthesis or signaling by silencing of *FaNCED1* or *FaPYR1*, respectively, inhibits fruit ripening in octoploid strawberry (*Fragaria* × *ananassa*)[4,8], a typical non-climacteric fruit, but the underlying mechanisms and how ABA signaling integrates with other intrinsic cues to coordinately regulate fruit ripening remain elusive.

N^6-methyladenosine (m^6A) is the most prevalent chemical modification in eukaryotic mRNAs[9,10]. It may impact mRNA metabolism, including mRNA stability, splicing, translation efficiency, and nuclear export[11–13], therefore affecting multiple biological pathways. As a dynamic and reversible post-transcriptional modification, m^6A is installed by the methyltransferase complex (writer) and removed by the demethylase (eraser), which belongs to the AlkB family of proteins[14,15]. Recognition of m^6A is achieved by the "reader" proteins, such as YTH-domain family proteins and specific RNA binding proteins (RBPs)[16,17]. In plants, the m^6A methylation has been elucidated to regulate various developmental and biological processes, such as vegetative growth[18–20], floral transition[21,22], reproductive development[23,24], photomorphogenesis[25,26], circadian clock[27,28], and biotic and abiotic stress responses[29–32]. We previously uncovered that m^6A modification participates in the regulation of ripening in diploid strawberry (*Fragaria vesca*)[33] and tomato (*Solanum lycopersicum*)[34]. However, the mechanistic basis of m^6A-mediated ripening control is still not well understood. Moreover, how m^6A methylation is regulated remains obscure. Such information is critical for understanding the connections of m^6A with other regulatory pathways in controlling fruit ripening.

In the present work, we discovered that FvALKBH10B acts as a strawberry m^6A demethylase, whose expression is regulated by ABA through FvABF3. Mutation of *FvALKBH10B* via CRISPR/Cas9 gene editing system results in a delay in fruit ripening and global m^6A hypermethylation. We further established that FvALKBH10B-mediated m^6A demethylation stabilizes mRNA of *SEPALLATA3* (*FvSEP3*) encoding a transcription factor, which in turn regulates the expression of ripening-related genes. Our study reveals the FvABF3-FvALKBH10B-FvSEP3 regulatory cascade in the control of strawberry fruit ripening, highlighting the complex relationship between ABA, epigenetic regulators, and transcription factors during ripening.

Results

FvALKBH10B is a demethylase for mRNA m^6A demethylation in strawberry

We previous revealed that m^6A modification represents a common feature of mRNAs in fruits of diploid strawberry *F. vesca* and is highly enriched around the stop codon or within the 3′ untranslated region (UTR)[33]. During fruit ripening, m^6A depositions in these regions display a substantial decline on a large number of transcripts[33], but the mechanistic basis remains unknown. We hypothesize that this process is regulated by specific m^6A demethylase, which oxidatively reverses m^6A in mRNAs. To identify m^6A demethylase candidates in strawberry, we performed BLAST analysis, which predicted 9 potential orthologs of *Arabidopsis* AlkB homologs (ALKBHs)[35] (Supplementary Data 1). All these strawberry ALKBH members, named based on their phylogenetic relationships with *Arabidopsis* ALKBHs (Fig. 1a), possess an intact and highly conserved AlkB domain (Supplementary Fig. 1a) with Fe (II) binding sites and alpha-ketoglutaramate (α-KG) binding sites (Supplementary Fig. 1b). By mining the transcriptome data of our previous analysis[33], we found that, among the 9 strawberry *ALKBH* genes, only *FvALKBH10B*, the ortholog of *Arabidopsis ALKBH10B*[21], exhibited a dramatic increase during fruit ripening, and this was confirmed by RT-qPCR (Fig. 1b; Supplementary Fig. 2a, b). It should be noted that no significant decrease in gene expression of m^6A writers, including the methyltransferases MTA and MTB, was observed during fruit ripening, indicating that the decline in m^6A deposition in this process is not regulated by m^6A writers (Supplementary Fig. 2c).

Sequence alignment confirmed the existence of AlkB domain in FvALKBH10B as that in *Arabidopsis* ALKBH10B and mouse ALKBH5, the reported m^6A demethylases[14,21] (Fig. 1c). To determine if FvALKBH10B possesses demethylation activity, the MBP-tagged FvALKBH10B (MBP-FvALKBH10B) recombinant protein was incubated with a synthetic 16 nucleotide-long m^6A-modified ssRNA. Liquid chromatography-tandem mass spectrometry (LC-MS/MS) analysis of the nucleosides digested from the reaction products revealed that more than 50% of the methyls in m^6A were effectively removed by the recombinant FvALKBH10B (Supplementary Fig. 3a) compared to the control, concomitant with a corresponding increase in adenosine (A) (Fig. 1d), indicating that FvALKBH10B has m^6A demethylation activity in vitro. To explore the oxidative demethylation activity of FvALKBH10B in vivo, HA-tagged FvALKBH10B (FvALKBH10B-HA) was transiently expressed in *Nicotiana benthamiana* leaves, and the full-length mRNAs were then isolated for LC-MS/MS detection of overall m^6A levels. The expression of FvALKBH10B resulted in a decrease in total m^6A levels (Fig. 1e), confirming the demethylation activity of FvALKBH10B in vivo.

Subcellular localization analysis showed that an enhanced green fluorescent protein (eGFP)-tagged FvALKBH10B (eGFP-FvALKBH10B) driven by its native promoter produced fluorescent signals in the cytoplasmic structure (Fig. 1f). Moreover, the fluorescent signals of eGFP-FvALKBH10B co-localized with those of a mCherry-tagged histone H2B (H2B-mCherry), a nucleus marker[36]. These results suggest that FvALKBH10B was localized in both cytoplasm and nucleus. Together, our data indicate that FvALKBH10B is an m^6A demethylase that functions in both cytoplasm and nucleus to demethylate mRNA m^6A modifications.

FvALKBH10B is induced by ABA and transcriptionally activated by FvABF3

During the development and ripening of strawberry fruit, the concentration of ABA gradually increases[37]. This, together with the observation that *FvALKBH10B* increases markedly in the ripening process (Fig. 1b), promoted us to hypothesize that *FvALKBH10B* expression may be regulated by ABA. As expected, *FvALKBH10B* was strongly induced by exogenous application of ABA (Fig. 2a), concomitant with a substantial decrease in overall m^6A levels (Fig. 2b). To explore how *FvALKBH10B* expression is regulated by ABA, its promoter sequence was submitted to PlantRegMap (http://plantregmap.gao-lab.org/regulation_prediction.php), which predicted ABF3, a master transcription factor in ABA signaling, as a potential upstream regulator. Strawberry *ABF3* (*FvABF3*) appeared to be ABA-responsive (Fig. 2c). There exist 4 ABRE *cis*-elements, the ABF3 binding motifs, in the promoter region (2.0 kb upstream of the start codon) of *FvALKBH10B*. Yeast one-hybrid (Y1H) indicated that FvABF3 binds to the promoter of *FvALKBH10B* (Fig. 2d). Moreover, the electrophoretic mobility shift assay (EMSA) showed a distinct band shift was observed when the purified recombinant FvABF3 protein (Supplementary Fig. 3b) was mixed with the biotin-labeled probe (30-mer oligo-nucleotide) containing the ABRE element (Fig. 2e). The shifted band was out-competed by the addition of excess unlabeled probe with intact ABRE element (cold probe), but not by a probe with mutated ABRE element (mutant cold probe) (Fig. 2e), confirming the binding of FvABF3 to the promoter of *FvALKBH10B* in vitro. Finally, to investigate whether FvABF3 directly binds to the promoter of *FvALKBH10B* in vivo, we performed a chromatin immunoprecipitation (ChIP) assay. For that purpose, an HA-tagged FvABF3 (FvABF3-HA) was overexpressed in diploid strawberry *F. vesca*, and the cross-linked DNA-protein complexes were captured by immunoprecipitation with anti-HA magnetic beads. Significant enrichment for the promoter region of *FvALKBH10B* containing the ABRE element was observed in FvABF3-bound chromatin (Fig. 2f), indicating that FvABF3 binds to *FvALKBH10B* promoter in vivo.

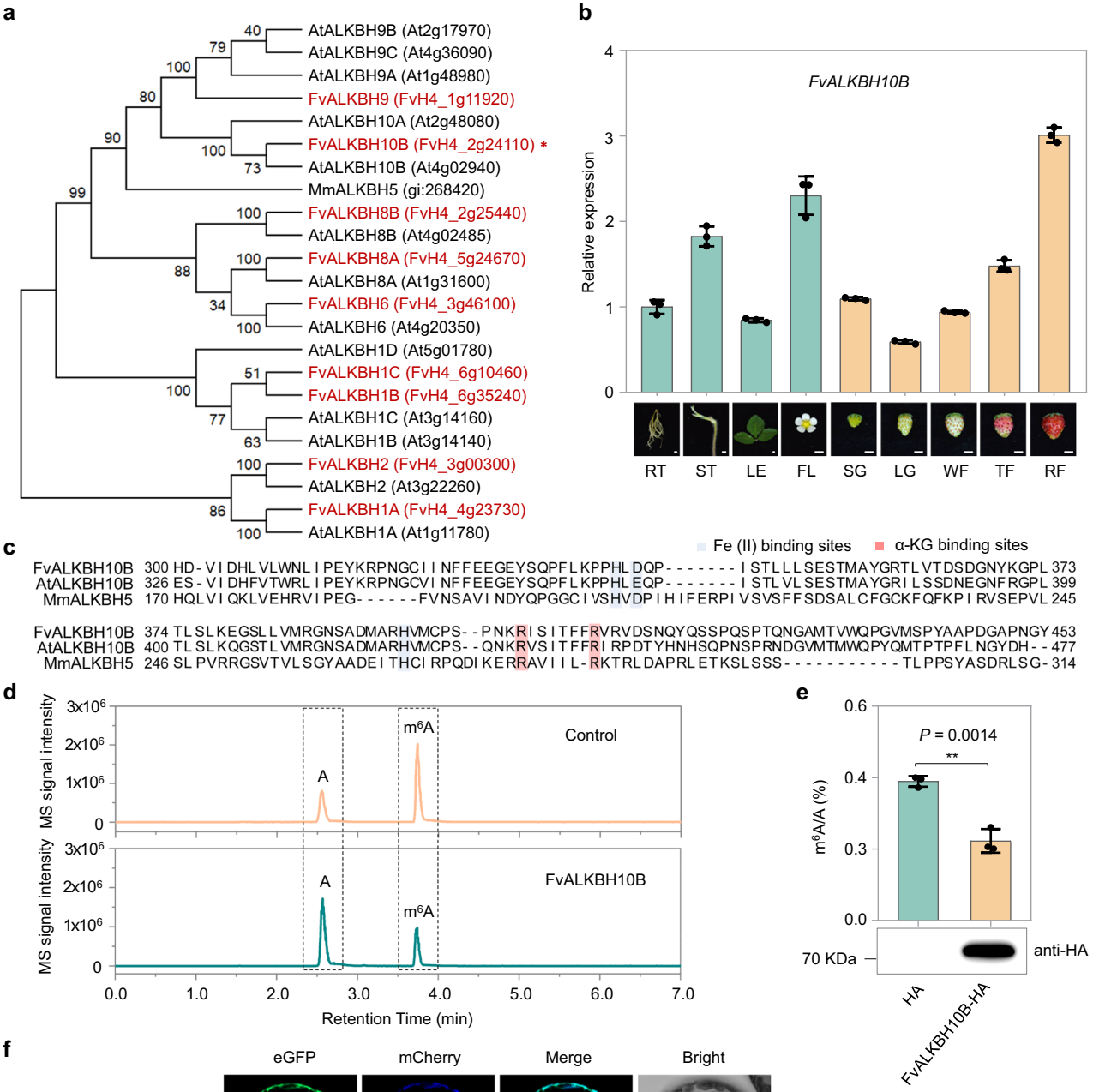

We next carried out a dual-luciferase reporter analysis in *N. benthamiana* leaves by co-expressing a reporter containing the *FvALKBH10B* promoter region fused with the *firefly luciferase (LUC)* reporter gene and an effector harboring the *FvABF3* coding sequence driven by CaMV35S. As shown in Fig. 2g, FvABF3 activated the expression of *FvALKBH10B*, which was indicated by an increase in relative LUC to renilla luciferase (REN) ratio in *N. benthamiana* expressing *FvABF3* compared to that expressing the empty effector (negative control). We then transiently silenced (via RNA interference; RNAi-*FvABF3*) and overexpressed (*35S:FvABF3*) *FvABF3* in strawberry fruits and observed a delay in fruit ripening in *FvABF3*-RNAi fruits and an acceleration in *35S:FvABF3* fruits (Fig. 2h, i). Consistent with these results, anthocyanin contents were significantly reduced in RNAi-*FvABF3* fruits and increased in *35S:FvABF3* fruits (Fig. 2j, k). Moreover, silencing of *FvABF3* decreased the expression of *FvALKBH10*, while overexpression of *FvABF3* exhibited an opposite effect (Fig. 2l, m).

Fig. 1 | FvALKBH10B has m^{6}A demethylase activity. a Phylogenetic analysis of strawberry ALKBH proteins. An unrooted neighbor-joining tree was generated by MEGA (version 6). The bootstrap supporting values is showed next to the nodes (1000 replicates). Species names are abbreviated as follows: Mm *Mus musculus*, At *Arabidopsis thaliana*, Fv *Fragaria vesca*. **b** Expression pattern of *FvALKBH10B* as determined by RT-qPCR. RT root, ST stem, LE leaf, FL flowers, SG small green, LG large green, WF white fruit, TF turning fruit, RF red fruit. Values are means ± standard error of mean (SEM) ($n = 3$ biological replicates), in which *ACTIN* (FvH4_6g22300) was used as an internal control. **c** Sequence alignment of the highly conserved AlkB domain in FvALKBH10B, *Arabidopsis* ALKBH10B (AtALKBH10B), and mouse ALKBH5 (MmALKBH5B). Highlighted by blue and pink rectangles are Fe (II) binding sites and alpha-ketoglutaramate (α-KG) binding sites, respectively. **d** Recombinant FvALKBH10B protein demethylates the m^{6}A modification in m^{6}A-containing ssRNA probe in vitro. LC-MS/MS chromatograms of digested m^{6}A-containing ssRNA are shown. **e** FvALKBH10B demethylates m^{6}A modification in mRNA in vivo. The mRNAs isolated from *Nicotiana benthamiana* leaves transiently expressing the FvALKBH10B-HA protein or the empty plasmid control (HA) were used for measurement of m^{6}A contents by LC-MS/MS. Values are means ± SEM ($n = 3$ biological replicates). Asterisks indicate significant differences (unpaired two-sided *t*-test; $^{**}P < 0.01$). Immunoblot analysis was performed to detect the expression of FvALKBH10B-HA fusion protein. **f** Subcellular location showing that FvALKBH10B locates in both cytoplasm and nucleus. *N. benthamiana* protoplasts co-expressing *eGFP* and *mCherry* were used as the negative control. The histone H2B serves as a nucleus marker. Protoplasts of the *N. benthamiana* leaves transiently co-expressing *eGFP-FvALKBH10B* and *H2B-mCherry* were isolated and observed under a Zeiss confocal microscopy. The experiment was repeated independently three times with similar results, and one representative result is shown. Scale bar = 10 μm. Source data are provided as a Source Data file.

Together, these data suggest that ABA promotes *FvALKBH10B* transcription through FvABF3, which positively regulates fruit ripening and binds directly to the promoter of *FvALKBH10B* and transcriptionally activates its expression.

FvALKBH10B affects the normal ripening of strawberry fruit

To determine the physiological role of FvALKBH10B, we generated stable *Fvalkbh10b* knockout mutants in diploid strawberry, *F. vesca* variety Ruegen, using a CRISPR/Cas9 gene-editing system. Two single guide RNAs (sgRNAs) containing different target sequences (T1 and T2) were designed to specifically target the exons of *FvALKBH10B* (Fig. 3a). We obtained three independent homozygous mutant lines (*Fvalkbh10b-1*, *Fvalkbh10b-2*, *Fvalkbh10b-3*) in the second generation, which were verified by sequencing genomic regions flanking the target sites. Line *Fvalkbh10b-1* and *Fvalkbh10b-2* carry 1-bp insertion, respectively, while line *Fvalkbh10b-3* harbors 1-bp deletion (Fig. 3b). All mutants were predicted to cause premature termination of FvALKBH10B protein translation within the following 60-bp sequence of the editing sites, just before the AlkB domain. The potential off-target sites in the strawberry genome were predicted by CRISPR-P (version 2.0, http://crispr.hzau.edu.cn/cgi-bin/CRISPR2/CRISPR), and no editing events were observed in the 5 potential off-target sites (Supplementary Fig. 4a, b), indicating the specific mutation for *FvALKBH10B*.

FvALKBH10B mutation led to elevated m^{6}A levels in total mRNA (Fig. 3c), confirming the in vivo m^{6}A demethylation activity of FvALKBH10B. All three mutant lines (*Fvalkbh10b-1*, *Fvalkbh10b-2*, and *Fvalkbh10b-3*) displayed an obvious petal non-shedding phenotype, i.e. the fruits retained the petals throughout the whole ripening process (Fig. 3d). This may be related to the effect of FvALKBH10B on floral transition as previously reported in *Arabidopsis*[21]. Intriguingly, the mutant lines showed similar and obvious ripening-delayed phenotypes (with petals artificially removed; Fig. 3e). A visible color change was observed at 27 days post anthesis (DPA) in fruits of the wild type, while the fruits in the *Fvalkbh10b* lines remained green at this stage (Fig. 3e). At 33 DPA, when the fruits in the wild type turned to a fully red color, the fruits from the mutants were only just starting to change color. Consistent with the color phenotype, the anthocyanin content was significantly decreased in fruits of the *Fvalkbh10b* lines (Fig. 3f). Moreover, the fruits in the mutants exhibited significantly lower levels for the major sugars, including sucrose, glucose, and fructose compared to the wild type (Fig. 3g–i). Notably, exogenous application of ABA could not rescue the delayed ripening phenotype of the *Fvalkbh10b* mutants, indicating that FvALKBH10B mediates the effect of ABA to regulating strawberry fruit ripening (Supplementary Fig. 5).

To confirm the positive role of FvALKBH10B in the regulation of fruit ripening, we also generated stable *FvALKBH10B* overexpression lines (*FvALKBH10B*-OE-L1 and *FvALKBH10B*-OE-L2) in diploid strawberry. These overexpression lines, which exhibited declined m^{6}A levels in total mRNA (Fig. 3j), showed phenotypes opposite to those seen in the *Fvalkbh10b* mutants (Fig. 3k, l). Compared to the control, the anthocyanin content was significantly increased in *FvALKBH10B*-OE fruits (Fig. 3m). Together, our data support the notion that FvALKBH10B is indispensable for the normal ripening of strawberry fruit.

FvALKBH10B mutation leads to global m^{6}A hypermethylation

To decipher the mechanisms by which FvALKBH10B regulates fruit ripening, we performed m^{6}A sequencing (m^{6}A-seq) and RNA sequencing (RNA-seq) using mRNA from fruits of wild-type and *Fvalkbh10b* mutant at 27 DPA. The libraries for sequencing were prepared with three replicates, in which the mRNA samples were independently prepared. Pearson correlation coefficient analysis between biological replicates confirmed the reliable repeatability of our m^{6}A-seq data (Supplementary Fig. 6a). A total of 30–32 million clean reads were produced for each library, of which 93–97% were mapped to the *F. vesca* Whole Genome v4.0.a2 (Supplementary Data 2). We identified 22012 m^{6}A peaks in common between the samples (Fig. 4a; Supplementary Data 3, 4), with 1954 peaks specific to the wild type (Fig. 4a; Supplementary Data 5) and 2856 peaks specific to the *Fvalkbh10b* mutant (Fig. 4a; Supplementary Data 6). The m^{6}A cumulative curve indicated that the overall m^{6}A level in *Fvalkbh10b* line was higher than that in wild type (Supplementary Fig. 6b), which was in accordance with the results observed in LC-MS/MS showing that mutation of *FvALKBH10B* led to elevated m^{6}A levels (Fig. 3c).

Most of the m^{6}A-containing transcripts (53.35% in wild type and 54.34% in *Fvalkbh10b* line) possess one m^{6}A peak, while some transcripts possess two or more m^{6}A peaks in wild type and the mutant (Fig. 4b). The metagenomic profiles of m^{6}A peaks in wild type and *Fvalkbh10b* line indicated that the m^{6}A modifications were highly enriched around both the start and stop codons and within the 3′ UTR (Fig. 4c). We divided the transcripts into 5 non-overlapping segments and found the m^{6}A peaks were most abundant around stop codon (39.71% in wild type and 40.27% in *Fvalkbh10b*), followed by 3′ UTR (23.13% in wild type and 23.14% in *Fvalkbh10b*), coding sequence (CDS) (17.67% in wild type and 17.68% in *Fvalkbh10b*), start codon (15.11% in wild type and 14.43% in *Fvalkbh10b*), and least abundant in 5′ UTR (4.38% in wild type and 4.48% in *Fvalkbh10b*) (Fig. 4d, e). After segment normalization by the relative fraction that each segment occupied in the transcriptome, the m^{6}A modifications in wild type and *Fvalkbh10b* line were exclusively enriched around the start and stop codons and within the 3′ UTR (Fig. 4f, g). We next examined the sequence motifs within the m^{6}A peaks and identified two typical m^{6}A consensus sequences (Fig. 4h), the RRACH (R = A/G; H = A/C/U) found in plants[10] and animals[38] and the URUAY (Y = C/U) specific for plants[39].

Subsequently, we explored the differential m^{6}A peaks and identified 2072 hypermethylated peaks and 1298 hypomethylated peaks, covering 1859 and 1200 genes, respectively, in the *Fvalkbh10b* mutant (Fig. 4i; Supplementary Data 7). The m^{6}A modification has been shown to affect mRNA abundance[34,40,41]. Our parallel RNA-seq analysis

https://doi.org/10.1038/s41467-024-55294-8

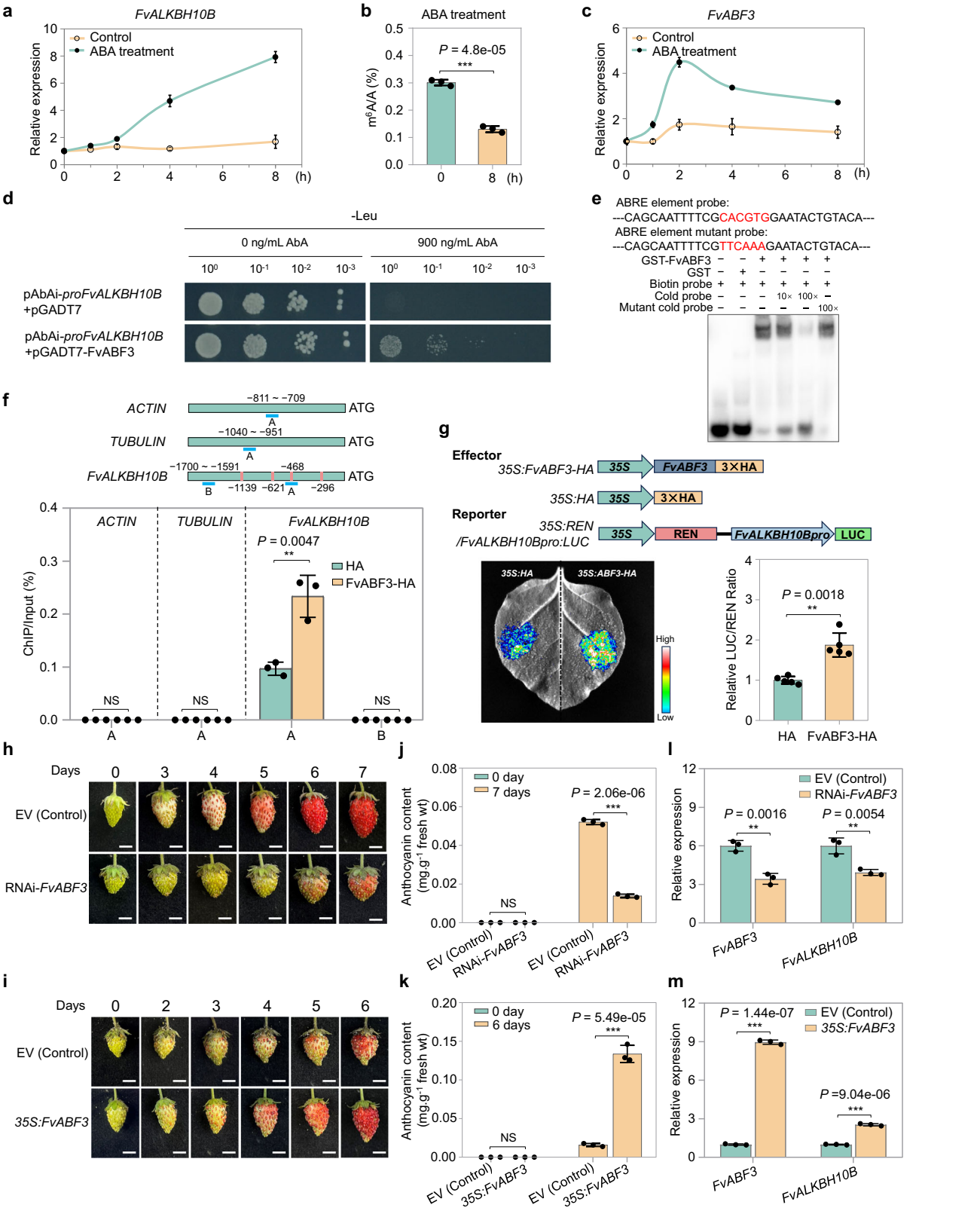

identified 3563 upregulated (Log_2(fold-change [FC]) ≥ 1; *P* value < 0.05) and 1365 downregulated (Log_2(FC) ≤ − 1; *P* value < 0.05) genes in the *Fvalkbh10b* mutant relative to the wild type (Fig. 4j, Supplementary Data 8). To assess if the changes in m^{6}A modification caused by *FvALKBH10B* disruption influences mRNA abundance, we compared the differentially expressed genes with the 1859 m^{6}A hypermethylated genes, which led to the identification of 588 overlapping genes (Fig. 4k; Supplementary Data 9). Among them, 324 genes (55.1%) were expressed at higher levels and 264 genes (44.9%) were expressed at lower levels in the *Fvalkbh10b* mutant (Fig. 4k). Together, our data suggest that loss of *FvALKBH10B* function results in global m^{6}A hypermethylation, which in turn leads to the changes in mRNA levels.

Fig. 2 | ABA induces the expression of *FvALKBH10B* through FvABF3 in strawberry. a The changes in gene expression of *FvALKBH10B* in response to ABA (50 μM) in strawberry fruits at large green stage as determined by RT-qPCR. *ACTIN* was used as an internal control. **b** LC-MS/MS assay revealing the decrease in total m^{6}A levels after exogenous application of ABA in strawberry fruits at large green stage. **c** Expression pattern of *FvABF3* in response to ABA in strawberry fruits at large green stage. In **a**–**c**, fruit samples were treated with ABA for indicated times before sampling. **d** Y1H assay showing the binding of FvABF3 to the promoter fragment of *FvALKBH10B*. The empty pGADT7 was used as the negative control. AbA Aureobasidin. **e** EMSA reveals that FvABF3 directly binds to the ABRE *cis*-acing elements in the *FvALKBH10B* promoter. The probe sequences are shown, with red letters representing the intact or mutated ABRE elements. For **d**, **e**, the experiment was repeated independently three times with similar results. **f** ChIP-qPCR assay shows the direct binding of FvABF3 to the promoter of *FvALKBH10B*. Pink boxes, ABRE elements; blue lines, regions used for ChIP-qPCR. Negative controls (*ACTIN* and *TUBULIN*) are included. **g** Transcriptional activity assay of *FvABF3*. The reporter plasmid contains the *FvALKBH10B* promoter fused with *firefly luciferase* (*LUC*), with *renilla luciferase* (*REN*) as an internal control. A representative image is shown. **h**, **i** Representative images of strawberry fruits silencing (**h**) or overexpressing (**i**) *FvABF3*. Fruits at large green stage were used for agroinfiltration and considered as days 0. EV, empty vector. Scale bar, 0.5 cm. **j**, **k** Anthocyanin contents in fruits shown in **h** (**j**) and **i** (**k**). **l**, **m** The mRNA levels of *FvABF3* and *FvALKBH10B* in fruits at days 2 shown in **h** (**l**) and **i** (**m**), as determined by RT-qPCR. For **a**–**c, f**, and **j**–**m**, values are means ± SEM ($n = 3$ biological replicates). For **g**, values are means ± SEM ($n = 5$ biological replicates). Asterisks indicate significant differences (unpaired two-sided *t*-test; $^{**}P < 0.01$, $^{***}P < 0.001$). NS no significant. Source data are provided as a Source Data file.

FvALKBH10 affects mRNA abundance of ripening-related genes

Among the m^{6}A-hypermethylated genes with differential expression in the *Fvalkbh10b* mutant, some are relevant to fruit ripening, such as *SEPALLATA3* (*FvSEP3*)[42], *ABA-RESPONSIVE ELEMENT-BINDING PROTEIN 1* (*FvAREB1*)[43], and *DOMAINS REARRANGED METHYLASE3.1* (*FvDRM3.1*)[44] (Supplementary Data 9). *FvSEP3* encodes a MADS-box transcription factor positively regulates strawberry fruit development and ripening[42], while *FvAREB1* encodes a bZIP transcription factor in the ABA signaling pathway[43]. *FvDRM3.1* encodes a key enzyme in the RNA-directed DNA methylation (RdDM) pathway that is negatively correlated with strawberry fruit ripening[44]. *FvSEP3* and *FvAREB1* exhibited m^{6}A hypermethylation in the 3′UTR (Fig. 5a), whereas *FvDRM3.1*, which appeared to be *Fvalkbh10b*-specific (Supplementary Data 6), displayed m^{6}A peaks in the CDS region (Fig. 5a). The differential m^{6}A modification in these 3 genes was confirmed by m^{6}A-IP-qPCR analysis (Fig. 5b). The transcript level of *FvSEP3* declined significantly in the *Fvalkbh10b* mutant as revealed by RNA-seq (Fig. 5c) and RT-qPCR (Fig. 5d). Although the transcript level of *FvAREB1* exhibited no significant change in the *Fvalkbh10b* mutant in the RNA-seq analysis (Fig. 5c), it displayed a significant decrease in the *Fvalkbh10b* line in RT-qPCR (Fig. 5d). By contrast, the transcript level of *FvDRM3.1* showed a significant increase in the *Fvalkbh10b* mutant as revealed by RNA-seq (Fig. 5c) and RT-qPCR (Fig. 5d). Considering the m^{6}A hypermethylation of *FvSEP3* and *FvAREB1* in the 3′UTR and that of *DRM3.1* in the CDS region, it appears that, consistent with our previous observation[33], m^{6}A deposition in the 3′UTR decreases mRNA levels, while m^{6}A in the CDS exhibits the opposite effect. Notably, the m^{6}A levels or expression of several ethylene-related genes, including *FvACS1*, *FvACS4*, and *FvCTR1*, showed no significant changes in the *Fvalkbh10b* mutant, suggesting that FvALKBH10B-mediated fruit ripening of strawberry is not regulated by ethylene-dependent process (Supplementary Fig. 7).

To determine how m^{6}A modification affects mRNA abundance, we performed transcription inhibition assay by using actinomycin D, the transcription inhibiter. Compared to the wild type, the degradation rate of *FvSEP3* and *FvAREB1* was dramatically increased, while the degradation rate of *FvDRM3.1* was decreased in the *Fvalkbh10b* mutant after actinomycin D treatment (Fig. 5e). These data suggest that FvALKBH10-mediated m^{6}A demethylation affects mRNA abundance of ripening-related genes, probably due to the effect of m^{6}A modification on mRNA stability. We also examined the translation efficiency of *FvSEP3*, *FvAREB1, and FvDRM3.1*, which was determined by calculating the abundance ratio of mRNA in the polysomal RNA versus the total RNA[33]. Notably, *FvALKBH10B* mutation significantly enhanced the translation efficiency of *FvDRM3.1* mRNA, but showed no effects on that of *FvSEP3* or *FvAREB1* (Fig. 5f), demonstrating that FvALKBH10B-mediated m^{6}A demethylation modulates translation of *FvDRM3.1*, but not that of *FvSEP3* or *FvAREB1*. Collectively, our data suggest that FvALKBH10B may regulate strawberry fruit ripening by targeting ripening-related genes, leading to the changes in mRNA stability or translation efficiency of these genes.

FvALKBH10B-mediated m^{6}A demethylation regulates *FvSEP3* function by stabilizing its mRNA

FvSEP3 acts as an important positive regulator for strawberry fruit ripening, as mutation of *FvSEP3* resulted in a dramatic delay in ripening[42]. The expression of *FvSEP3* increased significantly during fruit ripening (Fig. 6a), similar to that of *FvALKBH10B*, suggesting that the ripening-inhibited phenotype observed in the *Fvalkbh10b* mutant may be partially attributed to the changes in *FvSEP3* abundance caused by *FvALKBH10B* disruption. Silencing of *FvSEP3* in the *Fvalkbh10b* mutant background by RNAi showed an obviously additive effect on ripening inhibition (Fig. 6b–d), while overexpression of *FvSEP3* reversed the delayed ripening phenotype of the *Fvalkbh10b* mutant (Fig. 6e–g), confirming that FvSEP3 may regulate fruit ripening downstream of FvALKBH10B. We next explored whether FvALKBH10B directly binds to the transcripts of *FvSEP3* using RNA immunoprecipitation (RIP). The FvALKBH10B-bound mRNAs were immunoprecipitated from fruits of the *Fvalkbh10b* mutant transiently expressing the HA-tagged FvALKBH10B protein (FvALKBH10B-HA), and this led to an enrichment of *FvSEP3* (Fig. 6h), suggesting the direct binding of FvALKBH10B to the *FvSEP3* transcript.

In the m^{6}A-seq analysis, we identified one m^{6}A peak within 3′UTR of the *FvSEP3* transcript (Fig. 5a). There are 13 m^{6}A sequence motifs in this m^{6}A-containing peak region (roughly 200 nt wide), including 5 RRACH consensus sequences and 8 URUAH sequences (Supplementary Fig. 8a). We applied SELECT assay, a method for detection of single m^{6}A locus[45], to determine the specific m^{6}A sites in *FvSEP3* transcript. This led to the identification of 4 m^{6}A sites, i.e. m^{6}A1016 within the RRACH motif and m^{6}A896, m^{6}A912, and m^{6}A1012 within the URUAH motif, which were mediated by FvALKBH10B (Supplementary Fig. 8b, c). To examine if these specific m^{6}A sites affects *FvSEP3* mRNA stability, the native cDNA fragment of *FvSEP3* (*FvSEP3-WT*) or the mutated form (*FvSEP3-Mu*) in which each of these 4 m^{6}A sites was individually mutated from A to guanosine (G) was transformed into fruits of *F. vesca*, and then the degradation rate of mRNAs was monitored. As shown in Fig. 7a, the mRNA of native *FvSEP3* (*FvSEP3-WT*) degraded quickly in the presence of actinomycin D. Mutation of m^{6}A896 (*FvSEP3-Mu896*), but not m^{6}A912 (*FvSEP3-Mu912*), m^{6}A1012 (*FvSEP3-Mu1012*), or m^{6}A1016 (*FvSEP3-Mu1016*), led to an increase in mRNA stability of *FvSEP3* (Fig. 7a), indicating that m^{6}A896 serves as the key site essential for *FvSEP3* stability. When *FvALKBH10B* was co-expressed with *FvSEP3-WT* in *F. vesca*, the degradation rate of *FvSEP3-WT* mRNA declined (Fig. 7b), concomitant with a significant decrease in m^{6}A enrichment of *FvSEP3* (Fig. 7c). Importantly, co-expression of *FvALKBH10B* with *FvSEP3-Mu896* further decreased the degradation rate of *FvSEP3* mRNA (Fig. 7b). These results demonstrated that FvALKBH10B-mediated m^{6}A demethylation at m^{6}A896 stabilizes *FvSEP3* mRNA.

To explore whether m^{6}A modification affects physiological function of FvSEP3 in vivo, we transiently expressed various constructs in fruits of the wild-type *F. vesca*: native *FvSEP3* (*FvSEP3-WT*) or its mutated form *FvSEP3-Mu896*, in which the key m^{6}A site (m^{6}A896) was

https://doi.org/10.1038/s41467-024-55294-8

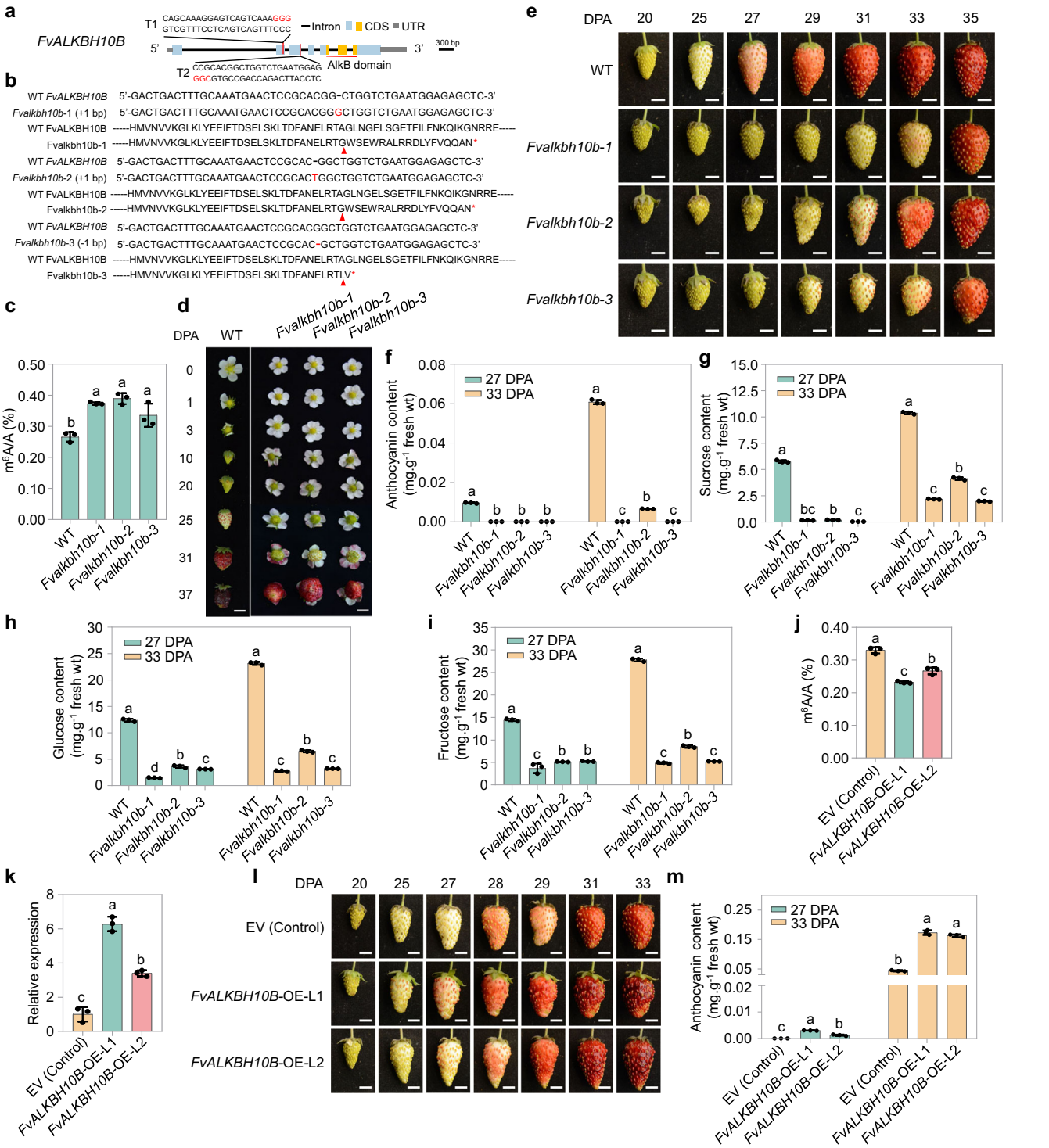

Fig. 3 | Mutation of *FvALKBH10B* leads to a delay in strawberry fruit ripening. **a** Schematic diagram of sgRNAs with two target sequences (T1 and T2) designed to specifically target the exons of *FvALKBH10B*. Red letters, protospacer adjacent motif (PAM); red vertical line, target sequence location; red horizontal line, Alkb domain location. **b** Genotyping of mutations mediated by CRISPR/Cas9 gene editing in the *Fvalkbh10b-1*, *Fvalkbh10b-2*, *Fvalkbh10b-3* mutant lines. Sequences of the isolated mutant alleles are aligned to the wild type (WT). The inserted/deleted nucleotides are colored with red to indicate the editing sites. Red arrowheads indicate the sites of frameshift in the translated mutant proteins. Red asterisks indicate protein translation termination site. **c** LC-MS/MS assay revealing the total m^{6}A level in fruits of WT and *Fvalkbh10b* mutants at 25 days post anthesis (DPA). **d**, **e** Phenotypes of strawberry flowers (**d**) and fruits (**e**) from WT and *Fvalkbh10b* mutants. Scale bar, 0.5 cm. **f**–**i** Changes in anthocyanin contents (**f**) and sugar contents, including sucrose (**g**), glucose (**h**), and fructose (**i**) in the mutant lines at 27 and 33 DPA. **j** LC-MS/MS assay revealing the changes in total m^{6}A level in fruits of overexpression lines (*FvALKBH10B*-OE) at 28 DPA. **k** Relative expression of *FvALKBH10B* in control and overexpression lines as determined by RT-qPCR. *ACTIN* was used as an internal control. **l** Phenotypes of fruit ripening in overexpression lines. EV empty vector. Scale bar, 0.5 cm. **m** Changes in anthocyanin contents in overexpression lines at 27 and 33 DPA. For **c**, **f**–**k**, and **m**, values are means ± SEM ($n = 3$ biological replicates). Data are analyzed using one-way ANOVA with Tukey's HSD test ($P < 0.05$). Different lowercase letters represent significant differences. Source data are provided as a Source Data file.

https://doi.org/10.1038/s41467-024-55294-8

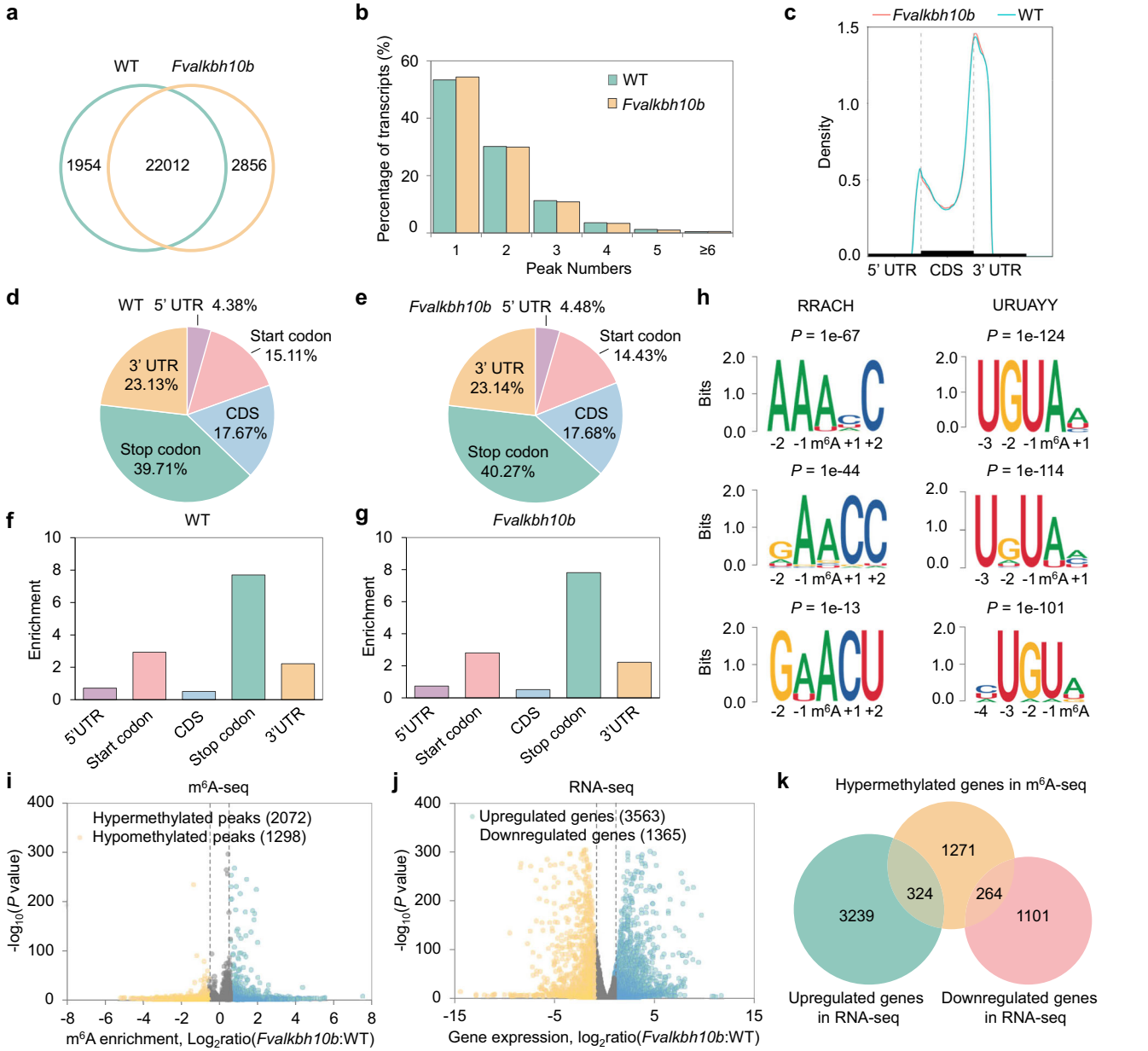

Fig. 4 | Changes in global m^{6}A methylation in fruits of *Fvalkbh10b* mutant. **a** Venn diagrams showing the number of common and specific m^{6}A peaks in the wild type (WT) and *Fvalkbh10b* mutant identified by m^{6}A-seq. **b** Percentage of the m^{6}A-modified transcripts with various m^{6}A peak numbers. **c** Metagenomic profiles of m^{6}A peak distribution along transcripts in WT and *Fvalkbh10b*. UTR untranslated region, CDS coding sequence. **d**–**g** The percentage (**d**, **e**) and relative enrichment (**f**, **g**) of m^{6}A peaks in five non-overlapping transcript segments. **h** Consensus motifs identified within m^{6}A-containing peak regions by HOMER. **i** Volcano plot showing hypermethylated (blue) and hypomethylates (yellow) m^{6}A peaks in fruits of *Fvalkbh10b* mutant across three biological replicates (fold change ≥ 1.5 and *P* value < 0.05; two-sided Wald test). The gray plot depicts the peaks with no significant difference. **j** Volcano plots revealing the upregulated (blue) and downregulated (yellow) genes in fruits of *Fvalkbh10b* mutant compared to WT by RNA-seq (fold change ≥ 2.0 and *P* value < 0.05; two-sided Exact test). **k** Venn diagram showing the overlap between differentially expressed genes and m^{6}A-hypermethylated genes. Source data are provided as a Source Data file.

mutated to G. As shown in Fig. 7d–f, overexpression of *FvSEP3-WT* accelerated fruit ripening, confirming the function of FvSEP3 in controlling ripening. Compared to the fruits overexpressing *FvSEP3-WT*, fruits overexpressing *FvSEP3-Mu896* ripened more quickly (Fig. 7d), accompanied by higher levels of anthocyanin (Fig. 7f). These results indicate that m^{6}A modification in *FvSEP3* regulates its function.

To further confirm that m^{6}A methylation regulates the function of FvSEP3 in the control of strawberry fruit ripening, either native *FvSEP3* (*FvSEP3-WT*) or the mutated form (*FvSEP3-Mu896*) was transiently expressed in fruits of the *Fvsep3* mutant (kindly provided by Dr. Chunying Kang from Huazhong Agricultural University). The *Fvsep3* mutant harbors a point mutation in *FvSEP3* causing a single amino acid G to E conversion in the conserved MADS domain, which leads to a significant delay in fruit ripening[42]. We found that native *FvSEP3* rescued the delayed ripening phenotype of the *Fvsep3* mutant (Fig. 7g–i). By contrast, fruits of the *Fvsep3* mutant transiently expressing *FvSEP3-Mu896* ripened faster than those expressing native *FvSEP3* (Fig. 7g–i). Together, these findings suggest that FvALKBH10B-mediated m^{6}A modification plays a critical role in the regulation of FvSEP3 function in strawberry.

FvSEP3 directly targets numerous genes relevant to fruit ripening

Although FvSEP3 plays a critical role in the control of strawberry fruit ripening[42], the mechanisms underlying FvSEP3-mediated

https://doi.org/10.1038/s41467-024-55294-8

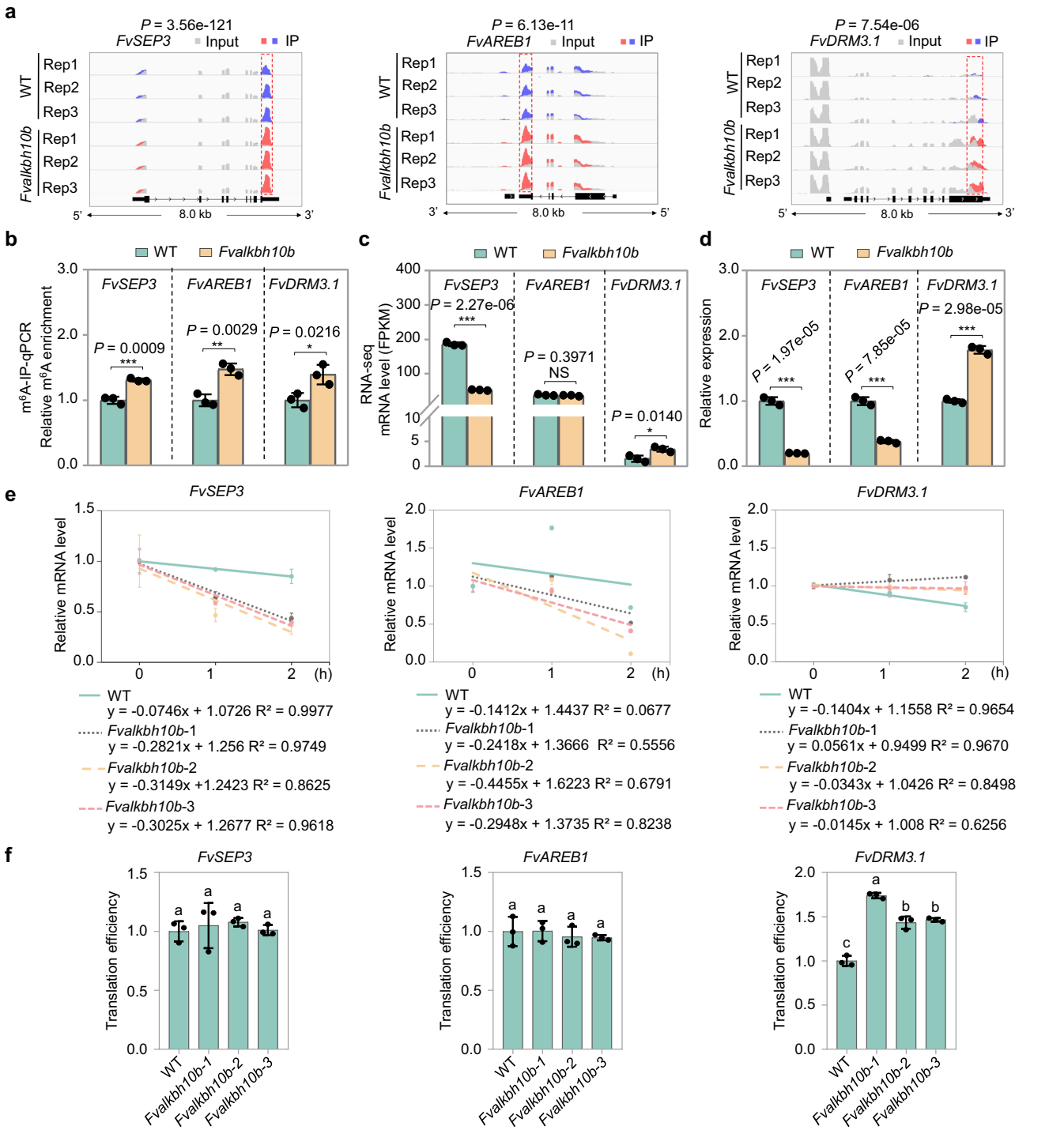

Fig. 5 | FvALKBH10B regulates mRNA abundance of ripening-related genes in strawberry. a Integrative Genomics Viewer (IGV) tracks showing the distribution of m^{6}A reads in transcripts of *FvSEP3*, *FvAREB1*, and *FvDRM3.1*. The red dot line rectangles indicate the position of m^{6}A peaks with significantly increased m^{6}A enrichment (*P* value < 0.05; two-sided Wald test) in fruits of *Fvalkbh10b* mutant compared to wild type (WT). **b** Validations of the m^{6}A enrichment by m^{6}A-immunoprecipitation (IP)-qPCR. **c**, **d** Transcript levels of the indicated genes determined by RNA-seq (**c**) and RT-qPCR (**d**). FPKM, fragments per kilobase of exon per million mapped fragments. *ACTIN* was used as an internal control in RT-qPCR analysis. **e** Transcription inhibition assay for the indicated genes. The mRNAs were isolated from WT and *Fvalkbh10b* mutant treated with actinomycin D, and subjected to RT-qPCR analysis. **f** Translation efficiency assay for the indicated genes. Translation efficiency was expressed as the abundance ratio of mRNA in the polysomal RNA versus the total RNA. For **b**–**f**, data are presented as means ± SEM ($n = 3$ biological replicates). For **b**–**d**, asterisks indicate significant differences (unpaired two-sided *t*-test; *$P < 0.05$, **$P < 0.01$, ***$P < 0.001$). NS no significant. For **f**, data are analyzed using one-way ANOVA with Tukey's HSD test ($P < 0.05$). Different lowercase letters indicate significant differences. Source data are provided as a Source Data file.

transcriptional regulation remain unclear. We performed DNA affinity purification sequencing (DAP-seq)[46] to unravel FvSEP3 binding sites on a genome-wide scale. For that purpose, recombinant FvSEP3 fused to HaloTag sequence was used to purify sheared genomic DNA from fruits of *F. vesca*. Two independent biological replicates for DAP-seq and DNA "input" libraries were prepared for high-throughput sequencing. We consistently obtained a total of 13,283 enriched peaks, corresponding to 10,674 genes, in both biological replicates

https://doi.org/10.1038/s41467-024-55294-8

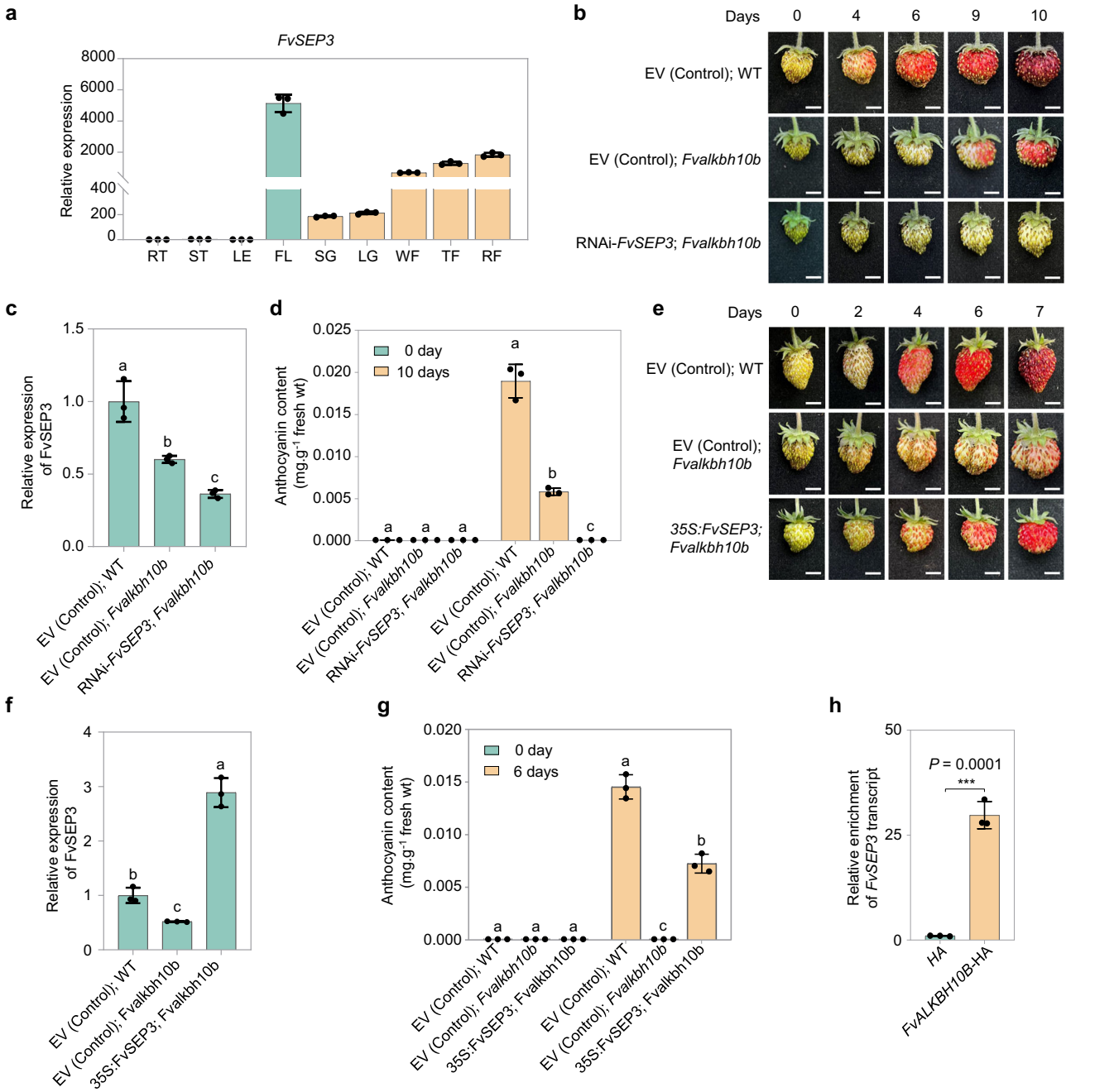

Fig. 6 | FvSEP3 regulates fruit ripening downstream of FvALKBH10B. a Gene expression of *FvSEP3* as determined by RT-qPCR. RT root, ST stem, LE leaf, FL flowers, SG small green, LG large green, WF white fruit, TF turning fruit, RF red fruit. *ACTIN* was used as an internal control. **b** Representative images of fruits silencing *FvSEP3* in the *Fvalkbh10b* mutant background. Fruits at large green stage were used for agroinfiltration and considered as days 0. EV empty vector, WT wild type. Scale bar, 0.5 cm. **c** The mRNA levels of *FvSEP3* in fruits shown in (**b**) as determined by RT-qPCR. **d** Anthocyanin contents in the fruits shown in **b**. **e**, Representative images of fruits overexpressing *FvSEP3* in the *Fvalkbh10b* mutant background. Fruits at large green stage were used for agroinfiltration and considered as days 0. Scale bar, 0.5 cm. **f** The mRNA levels of *FvSEP3* in fruits shown in (**e**), as determined by RT-qPCR. **g** Anthocyanin contents in the fruits shown in (**e**). **h** RNA immunoprecipitation (RIP) assay showing that FvALKBH10B directly binds *FvSEP3* transcript. The FvALKBH10B-HA fusion protein was transiently expressed in fruits of *Fvalkbh10b* mutant, and then the FvALKBH10B-bound mRNAs were immunoprecipitated and submitted to RT-qPCR assay. For **a**, **c**, **d**, and **f**–**h**, values are means ± SEM ($n = 3$ biological replicates). For **c**, **d**, **f**, and **g**, data are analyzed using one-way ANOVA with Tukey's HSD test ($P < 0.05$). Different lowercase letters indicate significant differences. For **h**, asterisks indicate significant differences (unpaired two-sided *t*-test; $^{***}P < 0.001$). Source data are provided as a Source Data file.

(Fig. 8a; Supplementary Fig. 9a; Supplementary Data 10–13). The binding sites were highly enriched around transcriptional start sites (TSS) (Fig. 8b; Supplementary Fig. 9b). A detailed analysis of the binding profiles indicated that 20.8% and 8.5% of the binding sites were located within promoter regions (up to 2.0 kb upstream from a TSS) and 5′UTRs (Fig. 8c), respectively, corresponding to a total of 3706 genes (Supplementary Data 14). The binding sites of FvSEP3 were distributed evenly across the length of all 7 *F. vesca* chromosomes (Supplementary Fig. 9c), suggesting that FvSEP3 has no preference for a specific chromosome.

A de novo motif prediction based on the FvSEP3-bound regions in the DAP-seq data showed the most enriched motif was represented by

https://doi.org/10.1038/s41467-024-55294-8

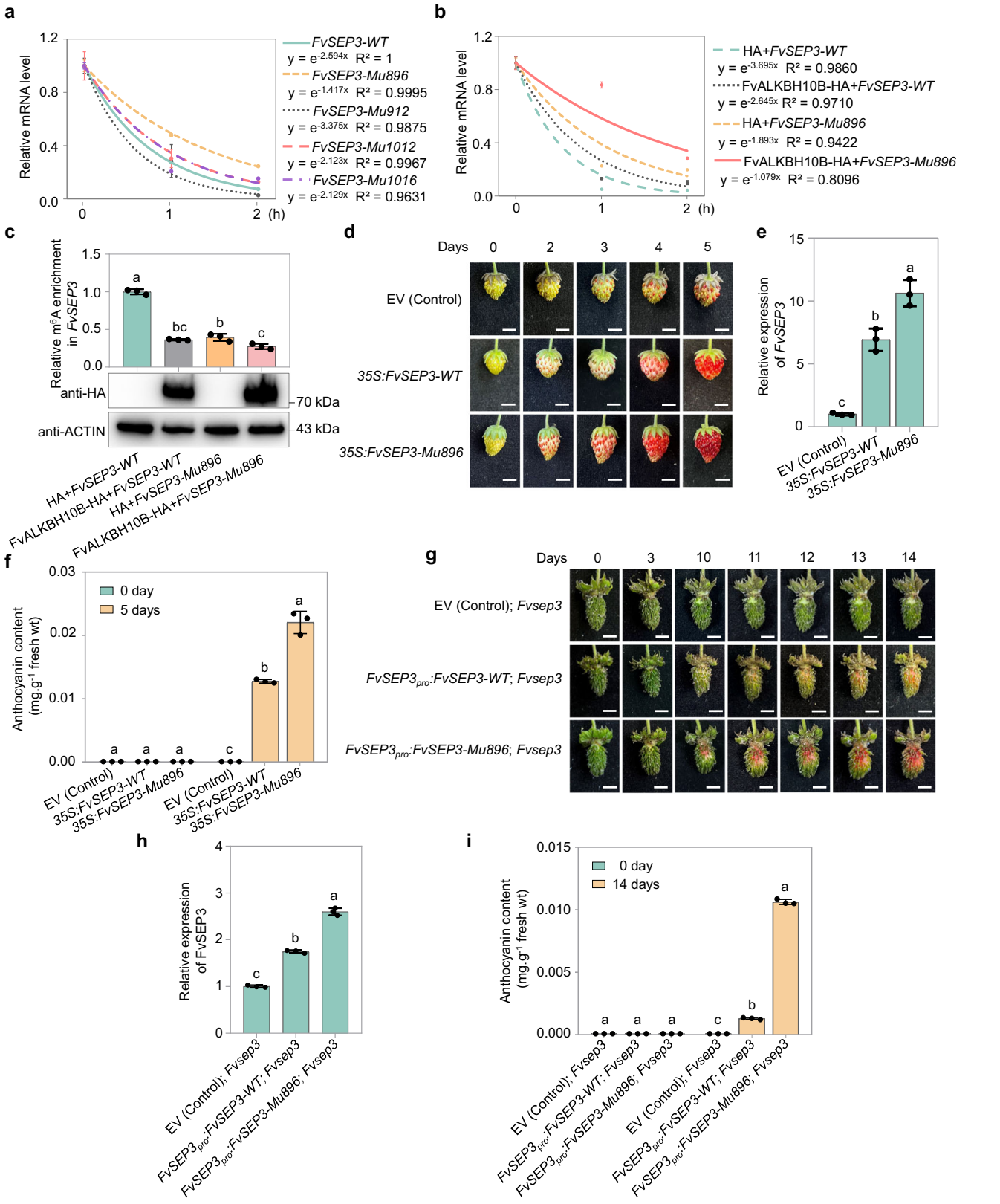

CCAWWWWAAG (W = A/T) (Fig. 8d), which is derived from a previously reported MADS-box recognition motif CArG-box[47]. Gene ontology (GO) enrichment analysis of the genes that contained FvSEP3 binding sites in promoter regions revealed a significant over-representation ($P < 0.05$; hypergeometric test) of catagories including "hormone-mediated signaling pathway", "fatty acid biosynthetic process", and "DNA binding and transcription regulation" (Fig. 8e), suggesting that FvSEP3 may directly control multiple biological pathways relevant to fruit ripening.

Subsequently, we compared the 10,671 FvSEP3 binding genes identified in our DAP-seq with the differentially expressed genes that have been previously revealed in the *Fvsep3* mutant[42]. A total of 1177

Fig. 7 | FvALKBH10B-mediated m^{6}A demethylation modulates *FvSEP3* function. **a** Determination of the *FvSEP3* mRNA stability. The native (*FvSEP3-WT*) or mutated *FvSEP3* (*FvSEP3-Mu*) cDNA fragment was transiently expressed in fruits of *F. vesca*. After actinomycin D treatment for 1 or 2 h, the total RNAs were extracted and subjected to RT-qPCR analysis. *ACTIN* gene severed as an internal control. **b** Influence of FvALKBH10B on *FvSEP3* mRNA stability. The native (*FvSEP3-WT*) or mutated *FvSEP3* (*FvSEP3-Mu896*) cDNA fragment was co-expressed with FvALKBH10B-HA or empty vector control (HA) in fruits of *F. vesca*. **c** m^{6}A-IP-qPCR assay showing the m^{6}A enrichment in *FvSEP3* transcript shown in **b**. Immunoblot analysis shows the FvALKBH10B-HA protein expression. **d** Representative images showing the fruits of the wild type transiently expressing the native (*FvSEP3-WT*) or mutated *FvSEP3* (*FvSEP3-Mu896*) cDNA fragment. Fruits at large green stage were used for agroinfiltration and considered as days 0. EV, empty vector. Scale bar, 0.5 cm. **e** The mRNA levels of *FvSEP3* in fruits shown in (**d**), as determined by RT-qPCR. **f** Anthocyanin contents in fruits shown in (**d**). **g** Representative images showing the fruits of the *Fvsep3* mutant transiently expressing the native (*FvSEP3-WT*) or mutated *FvSEP3* (*FvSEP3-Mu896*) cDNA fragment. Fruits at 30 days post anthesis were used for agroinfiltration and considered as days 0. Scale bar, 0.5 cm. **h** The mRNA levels of *FvSEP3* in fruits shown in (**g**), as determined by RT-qPCR. **i** Anthocyanin contents in fruits shown in (**g**). For **a**–**c**, **e**, **f**, **h**, and **i**, values are means ± SEM ($n = 3$ biological replicates). For **c**, **e**, **f**, **h**, and **i**, data are analyzed using one-way ANOVA with Tukey's HSD test ($P < 0.05$). Different lowercase letters indicate significant differences. Source data are provided as a Source Data file.

genes were identified in common, suggesting they are direct targets of FvSEP3 (Supplementary Data 15). Among them, 624 genes (53.0%) were considered as targets positively regulated by FvSEP3, as they were downregulated in the *Fvsep3* mutants, while 553 genes (47.0%) represented targets negatively regulated by FvSEP3, since they were upregulated in the *Fvsep3* lines.

Fruit development and ripening in strawberry are controlled by multiple phytohormones, of which auxin and gibberellic acid (GA) promote fruit development in the early stage[37], while ABA plays a central role in fruit ripening[4,5]. Interestingly, we identified multiple key genes in the biosynthetic pathway of auxin, GA, and ABA as direct targets of FvSEP3 (Supplementary Data 15), consistent with the role of FvSEP3 in the control of fruit development and ripening. We next selected 4 genes, i.e. *GH3.1*, *GA3ox1*, *NCED1*, and *CHS1*, which displayed FvSEP3 binding peaks in their promoter regions in the DAP-seq analysis (Fig. 8f), to validate their direct regulation by FvSEP3. *GH3.1* (encoding IAA-amido synthetase) and *GA3ox1* (encoding GA3-oxidase) participate in biosynthesis of auxin and GA[48,49], respectively, while *NCED1* (encoding *9-cis*-epoxycarotenoid dioxygenase) controls ABA biosynthesis[6]. FvCHS1 encodes chalcone synthase, a key enzyme responsible for anthocyanin biosynthesis[50].

To verify that FvSEP3 interacts with the promoter fragments of the selected genes, we performed an EMSA with purified recombinant FvSEP3 protein (Supplementary Fig. 3c). We observed a band shift for each promoter fragment when purified FvSEP3 protein was co-incubated with the biotin-labeled DNA probe (30-mer oligo-nucleotide) containing the CArG-box element (Fig. 8g), suggesting that FvSEP3 binds to the biotin-labeled promoter fragments. The shifted band was effectively competed by the addition of excess unlabeled DNA probe with intact CArG-box element (cold probe), but not by a probe with mutated CArG-box element (mutant cold probe) (Fig. 8g). These results indicated that FvSEP3 binds specifically to the promoters of *FvGH3.1*, *FvGA3ox1*, *FvNCED1*, and *FvCHS1* in vitro. Furthermore, we performed a ChIP assay to determine whether FvSEP3 directly binds to the promoters of the selected genes in vivo. The cross-linked DNA-protein complexes were enriched from fruits of *F. vesca* overexpressing an HA-tagged FvSEP3 (FvSEP3-HA). Specific enrichment for the promoter regions of *FvGH3.1*, *FvGA3ox1*, *FvNCED1*, and *FvCHS1* were observed in FvSEP3-bound chromatin (Fig. 8h), indicating that FvSEP3 binds to the promoter of these genes in vivo. Taken together, these data suggest that FvSEP3 regulates fruit development and ripening by directly targeting genes involved in biosynthesis of phytohormones and anthocyanins.

Based on our results presented in this study, we propose a model for strawberry fruit ripening governed by the FvABF3-FvALKBH10B-FvSEP3 regulatory cascade (Fig. 9). During the ripening of strawberry fruit, the accumulated plant hormone ABA activates the downstream transcription factor FvABF3, which directly binds to the ABRE *cis*-element in the promoter of the m^{6}A demethylase gene *FvALKBH10B* and promotes its expression. The induced FvALKBH10B stabilizes mRNAs of numerous ripening-related genes, including *FvSEP3*, by mediating their m^{6}A demethylation. In turn, FvSEP3 regulates fruit ripening by directly targeting ripening-related genes.

Discussion

The m^{6}A RNA demethylase responsible for the removal of m^{6}A has been characterized in various organisms. The fat mass and obesity-associated protein (FTO) and ALKBH5 represent the m^{6}A demethylases[14,51] in mammals. FTO affects human obesity and energy homeostasis[51], while ALKBH5 impacts mouse fertility[14]. In *Arabidopsis*, two m^{6}A RNA demethylases have been currently characterized, of which AtALKBH10B regulates floral transition[21], whereas AtALKBH9B affects the infectivity of RNA viruses[52] and promotes mobilization of a heat-activated long terminal repeat retrotransposon[30]. Here, we identified FvALKBH10B, the homolog of *Arabidopsis* AtALKBH10B, as a strawberry m^{6}A demethylase that oxidatively reverses m^{6}A methylation in mRNA in vitro and in vivo. We demonstrated that FvALKBH10-mediated m^{6}A demethylation promotes mRNA stability of *FvSEP3* and *FvAREB1*, but decreases mRNA stability of *FvDRM3.1*. The contrasting effect may be caused by different m^{6}A-binding proteins that recognize the specific sequence contexts around m^{6}A marks. We speculate that, similar to YTHDF2 in mammals[40], certain m^{6}A-binding proteins recognizing *FvSEP3* and *FvAREB1* interact with components in processing bodies (P-bodies), thereby promoting mRNA decay. On the contrary, another type of m^{6}A-binding proteins, resembling IGF2BPs in mammals[17] and ECT2 in *Arabidopsis*[41], recognize *FvDRM3.1*, leading to the delay in mRNA degradation, probably by disrupting the process of RNA decay in P-bodies. The detailed mechanisms deserve further investigation in the future.

We have speculated that FvALKBH10B may negatively regulate strawberry fruit ripening, since our previous work has shown that MTA, the m^{6}A methyltransferase, function as a positive ripening regulator in strawberry. Contrary to expectations, however, we observed that the *Fvalkbh10b* mutant lines exhibit a delay in fruit ripening, suggesting that FvALKBH10B plays a positive role in regulating fruit ripening. Consistent with this observation, we found that FvALKBH10B-mediates m^{6}A demethylation stabilizes mRNAs of ripening-related genes. We propose that the m^{6}A levels for specific ripening-related genes should be maintained at appropriate extent in strawberry to ensure fruit ripening. Disruption of MTA or FvALKBH10B may disturb the homeostasis of m^{6}A methylation of these genes and decrease their mRNA abundance, leading to the delay in fruit ripening. Notably, different mechanisms were utilized by MTA and FvALKBH10B to regulate fruit ripening in strawberry. MTA functions by facilitating mRNA stability of genes involved in ABA pathway including *NCED5*[33], while FvALKBH10B regulates fruit ripening mainly by stabilizing *FvSEP3* transcript (Figs. 6, 7). This may partially explain why both MTA and FvALKBH10B positively regulate strawberry fruit ripening. In fact, a similar phenomenon has also been observed in humans where both m^{6}A methyltransferase METTL3[53] and demethylase ALKBH5[54] promoted tumor growth and progression by modulating different genes. Notably, the expression of the homologous gene (FvH4_1g11920) of tomato *SlALKBH2*, which shows a sharp increase in the process of fruit ripening[34], remained relatively constant during strawberry fruit ripening (Supplementary Fig. 2a, b). It appears that this gene (FvH4_1g11920) does not contribute to the regulation of fruit ripening in strawberry. However, we cannot

https://doi.org/10.1038/s41467-024-55294-8

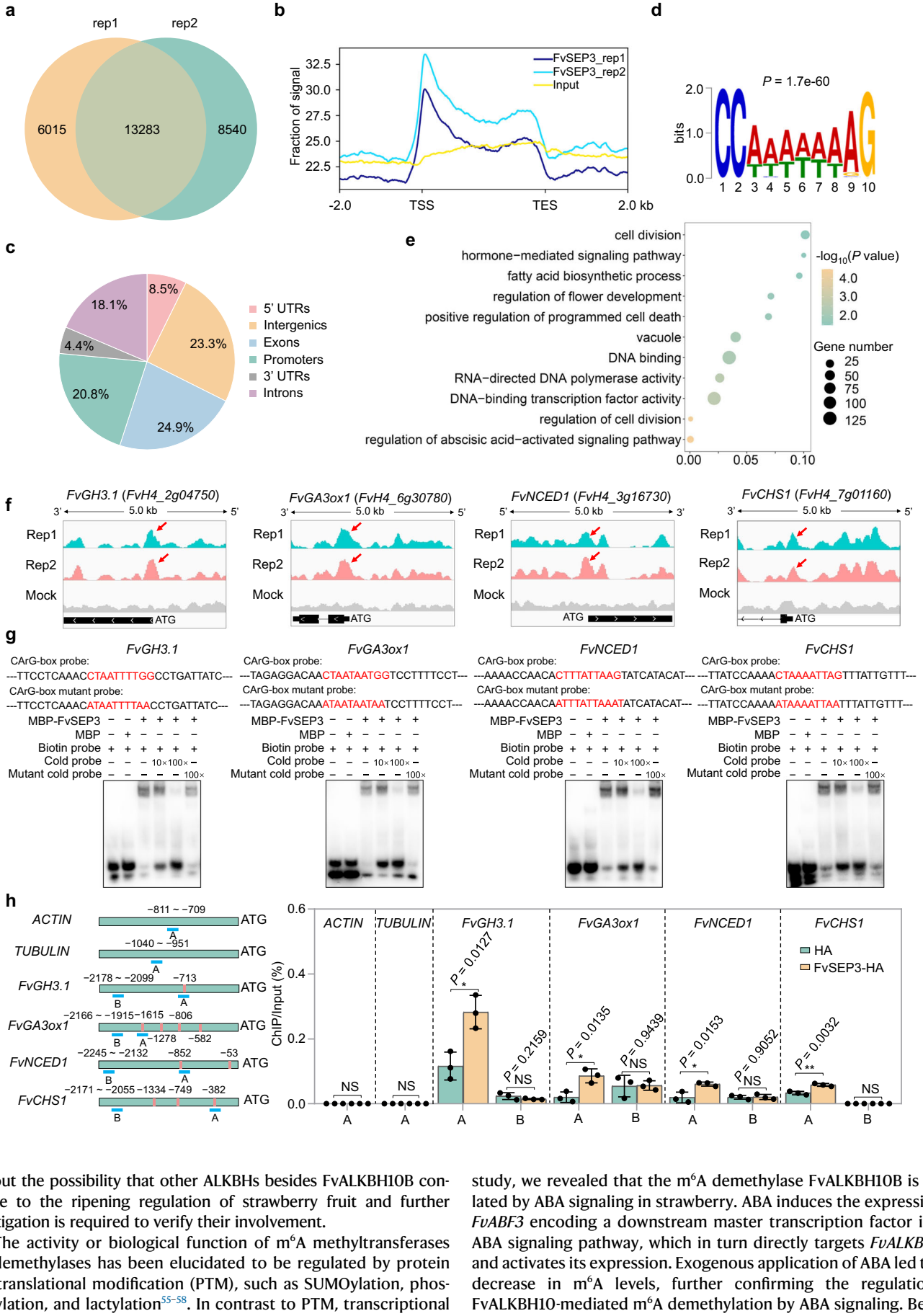

rule out the possibility that other ALKBHs besides FvALKBH10B contribute to the ripening regulation of strawberry fruit and further investigation is required to verify their involvement.

The activity or biological function of m^{6}A methyltransferases and demethylases has been elucidated to be regulated by protein post-translational modification (PTM), such as SUMOylation, phosphorylation, and lactylation[55–58]. In contrast to PTM, transcriptional regulation of m^{6}A machineries is poorly understood. In the present study, we revealed that the m^{6}A demethylase FvALKBH10B is regulated by ABA signaling in strawberry. ABA induces the expression of *FvABF3* encoding a downstream master transcription factor in the ABA signaling pathway, which in turn directly targets *FvALKBH10B* and activates its expression. Exogenous application of ABA led to the decrease in m^{6}A levels, further confirming the regulation of FvALKBH10-mediated m^{6}A demethylation by ABA signaling. Besides being critical for plant growth, development, and stress responses,

Fig. 8 | FvSEP3 directly targets genes involved in fruit ripening. a DAP-seq using two biological replicates (rep) identifies 13,283 high-confidence FvSEP3 binding peaks in the whole genome. **b** Metaplot of FvSEP3 binding sites. The FvSEP3 binding sites are centered on the TSS. TSS, transcription start site; TES transcription end site. **c** Distribution of FvSEP3 binding peaks across genomic features. **d** DNA logo of enriched DNA binding sites for FvSEP3. The *P*-value is provided. **e** Gene ontology (GO) enrichment for FvSEP3-bound genes determined by DAP-seq (One-sided hypergeometric test). Bigger dots represent more genes. **f** FvSEP3 binding peaks (Repeat 1 and 2) and negative control (mock) over the *FvGH3.1*, *FvGA3ox1*, *FvNCED1*, and *FvCHS1* loci as determined by DAP-seq. **g** EMSA reveals that FvSEP3 directly binds to the sequence motifs in the *FvGH3.1*, *FvGA3ox1*, *FvNCED1*, and *FvCHS1* promoters. The probe sequences are shown, with red letters representing the intact or mutated CArG-box elements. Recombinant purified FvSEP3 was incubated with biotin-labeled probe or unlabeled probe with intact (cold probe) or mutated (mutant cold probe) CArG-box elements. The experiment was repeated independently three times with similar results. **h** ChIP-qPCR assay shows the direct binding of FvSEP3 to the promoter of indicated genes. The promoter structures of the target genes are shown (left panel). Pink boxes, CArG-box elements; Green lines, regions used for ChIP-qPCR. Values are the percentage of DNA fragments that coimmunoprecipitated with anti-HA antibodies in fruits overexpressing FvSEP3-HA or HA control relative to the input DNAs (right panel). Negative controls (*ACTIN* and *TUBULIN*) are included. Values are means ± SEM ($n = 3$ biological replicates). Asterisks indicate significant differences (unpaired two-sided *t*-test; $^{*}P < 0.05$, $^{**}P < 0.01$). NS no significant. Source data are provided as a Source Data file.

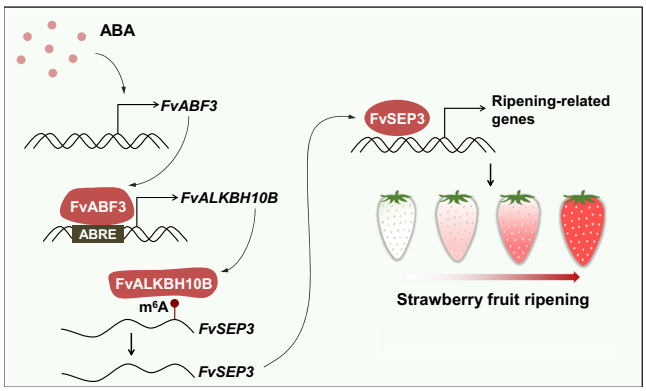

Fig. 9 | A proposed model for the regulation of fruit ripening by the FvABF3-FvALKBH10B-FvSEP3 cascade in strawberry. ABA activates the transcription of *FvABF3*, which in turn targets *FvALKBH10B* through the ABRE *cis*-element in the promoter and promote its expression. The enhanced FvALKBH10B stabilizes mRNAs of *FvSEP3* via m^{6}A-demethylation, which directly regulates ripening-related genes to control strawberry fruit ripening.

ABA serves as a dominant regulator of ripening and quality in non-climacteric fruits[4]. How ABA coordinates with other regulators such as epigenetic modifiers to regulate fruit ripening makes for an attractive research question. ABA signal transduction appears to be complicated and there exist two pathways, one of which is the "ABA-PYR/PYL-PP2C-SnRK2-ABF/AREB" core signaling network[59]. In this pathway, ABA signals are transmitted to downstream ABA-responsive genes through ABFs/AREBs, which belong to the basic-domain leucine zipper (bZIP) transcription factor[60]. There are 9 ABF/AREB homologs in the *Arabidopsis* genome[61] and FvABF3 appears to be the homolog of *Arabidopsis* ABF3. We propose that ABA regulates fruit ripening partially by reprogramming of m^{6}A epitranscriptome. Our study not only uncovers a previously unknown layer of regulation on m^{6}A methylation, but also reveals a mechanism underlying ABA-mediated ripening regulation.

The m^{6}A modification modulates multiple biological processes by affecting mRNA metabolism of key genes; for instance, m^{6}A on transcripts of *WUSCHEL* (*WUS*) and *SHOOTMERISTEMLESS* (*STM*), the key shoot meristem regulator genes, inversely correlates with their mRNA stability, thus regulating shoot stem cell fate[18]. m^{6}A also impacts mRNA stability of *FLOWERING LOCUS T* (*FT*), *SQUAMOSA PROMOTER BINDING PROTEIN LIKE 3* (*SPL3*), and *SPL9*, which encode the key flowering time regulators, thereby influencing floral transition[21]. Here, we showed that *FvSEP3*, a MADS-box gene critical for strawberry fruit development and ripening, is regulated by FvALKBH10B-mediated m^{6}A demethylation. FvALKBH10B binds directly to the transcript of *FvSEP3* and modulates its stability via m^{6}A demethylation. As a homolog of the *Arabidopsis SEP3*, *FvSEP3* belongs to the class E floral homeotic genes in the well-known ABCE model for flower development[42]. Other clades of the *SEP* genes, such as *MADS-RIN* in tomato, a *SEP1-like* gene, acts as a master regulator of tomato fruit ripening, which directly regulates the expression of key enzymes in the ethylene biosynthetic pathway[47]. In this study, we provide several lines of evidence that FvSEP3 directly modulates genes in the ABA and anthocyanin biosynthetic pathway, suggesting that FvSEP3 plays a direct role in the regulation of ABA biosynthesis and anthocyanin generation.

Considering that FvALKBH10B and its homologs from various non-climacteric fruits exhibit high similarity (Supplementary Fig. 10), we propose that the FvALKBH10B-mediated control of fruit ripening and the regulatory mechanism we describe here may exist in other non-climacteric fruits.

Methods

Plant materials and growth condition

Diploid strawberry *F. vesca* variety Ruegen was grown in a greenhouse under standard culture conditions or in a growth room under a 12-h-light/12-h-dark photoperiod with a light intensity of 200 − 300 μmol m^{-2} s^{-1} at 23 °C. Fruits were harvested at different development stages, including small green (SG, about 15 DPA), large green (LG, about 22 DPA), white fruit (WF, about 25 DPA), turning fruit (TF, about 27 DPA), and red fruits (RF, about 31 DPA). All fruit samples with achenes stripped were immediately frozen in liquid nitrogen and stored at −80 °C until use.

Strawberry ALKBHs identification and phylogenetic analysis

The amino acid sequences of *Arabidopsis* ALKBHs[35] were used as queries to search against the *F. vesca* reference genome database (https://www.rosaceae.org/species/fragaria_vesca/genome_v4.0.a2) by the BLASTP program with default parameters. Multiple sequence alignment was performed with the ALKBH protein sequences of *Arabidopsis*[35], mouse[14], and strawberry using ClustalX (version 2.1, http://www.clustal.org/clustal2/) with multiple alignment mode. The resulting alignment file was loaded into MEGA6 software (https://www.megasoftware.net/dload_win_gui) to construct a neighbor-joining (NJ) phylogenetic tree.

RNA isolation and RT-qPCR

Total RNAs were isolated from strawberry fruits using the plant RNA extraction kit (Magen, China, R4165-02). The extracted RNAs was digested with DNase I (Takara, D2215) and then reversely transcribed into cDNA using HiScript® III RT SuperMix for qPCR kit (Vazyme, China, R323-01). qPCR was carried out on a StepOnePlus Real-Time PCR System (Applied Biosystems, USA) with the following program: 95 °C for 30 s, followed by 40 cycles at 95 °C for 5 s and 60 °C for 30 s. The $2^{(-\Delta\Delta CT)}$ method was used for calculating the relative levels of gene expression[62]. Strawberry *ACTIN* (FvH4_6g22300) was applied to normalize the expression values. Three biological replicates were conducted and the primers are listed in Supplementary Data 16.

Quantitation of mRNA m^{6}A by LC-MS/MS

Total RNAs were extracted from three biological replicates of strawberry fruits or *N. benthamiana* leaves. Each replicate consisted of a

pool of ten fruits or six leaves collected from three plants. The mRNAs were isolated from total RNAs by the Dynabeads mRNA purification kit (Life Technologies, USA, 61006). Then, 200 ng of mRNAs from each sample were digested by 1 unit of nuclease P1 (Wako, Japan, 145-08221) at 37 °C for 6 h. The digested samples were separated using a UPLC (Waters, USA) equipped with an ACQUITY UPLC HSS T3 column (2.1 × 100 mm; 1.7 μm internal diameter). The mobile phase containing buffer A (0.1% formic acid in ultrapure water) and buffer B (100% acetonitrile) were performed at a 0.38 mL min^{-1} flow rate with the following buffer gradient: 1%/99% (A/B) at 0 min, 10%/90% at 4 min, 90%/10% at 8 min, and 1%/99% at 10 min. After separation, the nucleosides were detected by a Triple Quad Xevo TQ-S mass spectrometer (Waters, USA) using MassLynx software (version 4.1) with the following parameters: positive ion mode, capillary voltage, 3 kV; cone voltage, 25 V for adenosine (A) and 20 V for N^6-methyladenosine (m^6A); desolvation temperature, 400 °C; source temperature, 150 °C; desolvation gas flow, 800 L h^{-1}; collision gas flow, 0.14 mL min^{-1}; collision energy, 20 V. The nucleosides were quantified on basis of the nucleoside-to-base ion mass transitions from m/z 268.0 to 136.0 (A) and m/z 282.0 to 150.1 (m^6A)[33]. The pure commercial adenosine (A; TargetMol, China, T0853) and N^6-methyladenosine (m^6A; TargetMol, China, T6599) were employed to generate the standard curves, which were subsequently used to calculate the contents of A and m^6A in each sample by fitting the peak areas to the standard curves. The m^6A levels were presented in the form of m^6A/A ratio. The mass spectrometry data are provided in the Supplementary Data 17.

Demethylation activity assay

For demethylation activity assay in vitro, the coding sequence of *FvALKBH10B* was PCR-amplified and inserted into the pETMALc-H-MBP vector (Merck KGaA) to generate MBP-tagged FvALKBH10B (MBP-FvALKBH10B). The resulting vector was transformed into *Escherichia coli* strain BL21 (DE3) competent cells, which were then cultured at 16 °C for 18 h with induction of 1 mM isopropyl-1-thio-β-D-galactopyranoside (IPTG). To obtain recombinant MBP-ALKBH10B proteins, the bacterial cells were collected and lysed by ultrasonication, and the crude lysate was centrifuged at 12,000 × *g* for 10 min at 4 °C. The supernatant was subjected to a gravity-flow column filled with Amylose Resin (NEB, E8021V), and then the bound recombinant MBP-ALKBH10B proteins were eluted. To measure the demethylation activity, 20 μg of MBP-FvALKBH10B or MBP protein was incubated with 1 nM m^6A-containing ssRNA (AUUGUCAG[m^6A]CAGCAGC) at 25 °C for 1 h[21]. The ssRNA was purified from the mixtures and submitted to LC-MS/MS analysis as described above. All primers used for constructing vector are listed in Supplementary Data 16.

For demethylation assay in vivo, the coding region of *FvALKBH10B* was PCR-amplified from strawberry cDNA and inserted into the pCAMBIA1302 vector. The resulting construct and the empty vector were transformed into *A. tumefaciens* strain GV3101, which was used for transient transformation of *N. benthamiana* leaves[63]. The demethylation activity was detected by analyzing the abundance of mRNA m^6A in *N. benthamiana* leaves that transiently expressed *FvALKBH10B* or empty vector (control) using LC-MS/MS assay as describe above. The experiment was performed with 3 biological replicates. Primers are listed in Supplementary Data 16.

Western blot analysis

Proteins were separated by 10% SDS-PAGE and then electro-transferred onto an Immobilon-P PVDF membrane (Millipore, USA, IPVH00010). The membranes were blocked with 5% non-fat milk in 1× TBST buffer for 1 h at 25 °C, and then incubated with anti-HA (1:5000 dilution, MBL, M180), or anti-ACTIN (1:5000 dilution, Abmart, M001814) antibodies for 2 h. After washing three times by TBST buffer, the PVDF membrane was incubated with horseradish peroxidase (HRP)-conjugated anti-mouse IgG (1:5000 dilution, Abmart, M21002) secondary antibody for another 1 h. The immunoreactive bands were visualized by a chemiluminescence imaging system (5200 Multi, Tanon, China).

Subcellular localization

The promoter and coding sequence of *FvALKBH10B* were separately cloned from DNA or cDNA of *F. vesca* and insert into the pCAMBIA1302-eGFP vector to generate *FvALKBH10Bpro:eGFP-FvALKBH10B* construct. The resulting plasmid was introduced into *A. tumefaciens* strain GV3101, which was then injected into *N. benthamiana* leaves[63]. To obtain an accurate subcellular localization, the nucleus marker fused with *mCherry* (*H2B-mCherry*) was co-expressed with the *FvALKBH10Bpro:eGFP-FvALKBH10B*. After 42 h of infiltration at 22 °C, the mesophyll protoplasts were isolated[64] and visualized under a Zeiss ultra-high resolution confocal microscope (Zeiss, German, LSM 980 with Elyra7) at the excitation/emission wavelength of 488/510 nm (eGFP) or 587/610 nm (mCherry). Primers are listed in Supplementary Data 16.

ABA treatment

For gene expression and m^6A level analysis upon ABA treatment, the diploid strawberry fruits with achenes stripped were pre-cooled to 4 °C, sliced into 1 mm discs, and then incubated in equilibration buffer (50 mM MES, pH 5.5, 10 mM $MgCl_2$, 10 mM EDTA, 5 mM $CaCl_2$, and 5 mM Vc) with 200 mM mannitol for 30 min. The discs were then immersed in the equilibration buffer containing 50 μM ABA[65]. Discs incubated in the equilibration buffer with 200 mM mannitol served as control. After incubation for 0, 1, 2, 4, and 8 h, the discs were harvested and subjected to RT-qPCR and m^6A level analysis. For the phenotype observation of strawberry fruits after ABA treatment, fruits from the *Fvalkbh10b* mutants and the wild-type control were treated with 100 μM ABA every 2 days after pollination until turning stage[37].

Y1H analysis

Y1H assays were conducted according to the Matchmaker Gold Yeast One-Hybrid Library Screening System user manual (Clontech, USA). The coding sequence of *FvABF3* were amplified from cDNA of strawberry and ligated into the pGADT7 vector (Clontech, USA), while specific DNA sequences from promoter region of *FvALKBH10B* were amplified from genomic DNA of strawberry and inserted into the pAbAi vector (Clontech, USA). The resulting pAbAi construct was digested with *BstB1* or *BbS1* and then transformed into the yeast (*S. cerevisiae*) strain Y1H Gold, which was then plated on synthetic defined (SD)/−Ura agar medium. Primers used in vector construction are listed in Supplementary Data 16.

EMSA

The full-length coding sequence of *FvABF3* was inserted into the pGEX-6P-1-GST (GE Healthcare, USA) vector to generate the GST-FvABF3 recombinant protein, while that of *FvSEP3* was cloned into the pETMALc-H-MBP (Merck KGaA, Germany) vector to generate MBP-FvSEP3. The resulting vectors were separately transformed into *E. coli* strain BL21 or BL21 (DE3) competent cells, which were used for purification of recombinant proteins[34,66]. The 5′ biotin-labeled double-stranded DNA probes were prepared by annealing 5′ biotin-labeled oligonucleotides to the corresponding complementary strands. The purified recombinant proteins were incubated with biotin-labeled or unlabeled DNA probes for 20 min at 25 °C, and then the samples were separated by a 6% (w/v) native polyacrylamide gel. All primers used for vector construction and the oligonucleotide probes are listed in Supplementary Data 16.

ChIP assay

The coding sequence of *FvABF3* and *FvSEP3* was individually amplified from cDNA of *F. vesca* and separately ligated into the pCAMBIA1302

plasmid to generate *35S:FvABF3-HA* and *35S:FvSEP3-HA* vectors. The resulting constructs were individually transformed into the *A. tumefaciens* strain GV3101, which was subsequently infiltrated into fruits of *F. vesca* at large green stage[66]. The empty vector served as the control. For ChIP assay, the infiltrated fruits with achenes stripped were sliced and fixed in 1% (w/v) formaldehyde and then subjected to nuclear isolation[66]. The enriched nuclei were lysed to obtain the chromatin with an average size of 250 − 1500 bp. A small part of the sonicated chromatin was retained as the input sample, and the remaining fragmented chromatin was incubated with HA-Nanoab-Magnetic beads (Lablead, China, HNM-25-1000) at 4 °C for 4 h. Subsequently, the beads were collected, and the DNA-protein complexes were detached from the beads by rotation at 65 °C for 1 h. The cross-linking was then reversed by incubation at 65 °C for 12 h with the supplementation of NaCl at a final concentration of 200 mM. The immunoprecipitated DNA was recovered using a TIANquick Mini Purification Kit (TIANGEN, China, DP214) and subjected to qPCR analysis as described above. Values are expressed as the percentage of DNA fragments that coimmunoprecipitated with anti-HA antibodies in fruits overexpressing FvABF3-HA or HA control relative to the input DNAs. The primers used for ChIP assay are provided in Supplementary Data 16.

Dual-luciferase reporter assay

For dual-luciferase reporter assay, the coding sequence of *FvABF3* was inserted into the pCAMBIA1302 plasmid as effector, and the *FvALKBH10B* promoter was cloned into the pGreen-II-0800-LUC dual reporter vector. Both effector and reporter were co-transformed into the *N. benthamiana* leaves by using *Agrobacterium tumefaciens* strain GV3101. LUC and renilla (REN) luciferase activities were measured using the dual-luciferase reporter assay system (Promega, USA. E1910). The relative luciferase activity was presented by the representative image and calculated as the ratio of LUC to REN[67]. Primers are listed in Supplementary Data 16.

CRISPR/Cas9 and overexpression vector construction and plant transformation

Two specific sgRNAs targeting the coding region of *FvALKBH10B* was designed using CRISPR-P2.0 (http://crispr.hzau.edu.cn/cgi-bin/CRISPR2/CRISPR). The sgRNA expression cassettes that driven by the *AtU6-1* and *AtU3b* promoter, respectively, were amplified and inserted into the pYLCRISPR/Cas9Pubi-H binary vector using the Golden Gate method[68]. To construct the overexpression vector, the full-length coding sequence of *FvALKBH10B* was cloned from cDNA of the *F. vesca* fruits and insert into the pCAMBIA2300-eGFP vector.

The resultant constructs were separately transformed into *A. tumefaciens* strain GV3101. The *A. tumefaciens*-mediated transformation of diploid strawberry leaf discs was performed as previously reported[69]. To identify mutant genotypes, genomic DNA was extracted from homozygous mutant lines in the second generation. The genome regions containing the target sites and potential off-target sits were PCR-amplified and Sanger-sequenced. For transgenic overexpression plants, PCR genotyping was performed to amplify the flanking regions of the vector insertion site. All primers used for constructing vectors and screening the transgenic plants are listed in Supplementary Data 16.

Measurement of anthocyanin and soluble sugar

For anthocyanin measurement, the samples were subjected to high-performance liquid chromatography (HPLC) analysis on an ACQUITY UPLC system (Waters, USA) equipped with a C_{18} column according to the manufacturer's recommendations. Cyanidin-3-glucoside (C3G) was employed as standard[66].

For soluble sugar analysis, 0.5 g of fruit powder was added into 2.5 mL of double distilled water and incubated in a water bath for 30 min at 80 °C. The individual sugars (sucrose, glucose, and fructose) were identified and quantified using HPLC system (e2695, Waters, USA) equipped with a Waters 2414 RI detector. Each sample (10 μL) was injected onto a Sugar-Park™ I column (6.5 × 300 mm, Waters, USA) with a column temperature of 90 °C at a flow rate of 0.6 mL/min. D-(+) glucose, D-(−) fructose, and sucrose (Sigma-Aldrich, USA) were applied as standards for generating dose-response curves. There were three biological replicates and each sample contained five fruits from three plants.

m^{6}A-seq and RNA-seq

For m^{6}A-seq, total RNAs were extracted from fruits of wild type and the *Fvalkbh10b* mutant at 27 DPA. mRNAs were isolated from the qualified RNA samples and fragmented into ~100 nucleotide-long fragments. The cleaved mRNA fragments were incubated for 2 h at 4 °C with anti-m^{6}A polyclonal antibody (Synaptic Systems, German, 202003). NEBNext Ultra RNA library preparation kit (NEB, USA, E7530) was used for constructing the libraries from immunoprecipitated mRNAs or pre-immunoprecipitated mRNAs (input)[70]. Sequencing was carried out on the Illumina Novaseq™ 6000 platform with a paired-end read length of 150 bp. The sequencing reads from the input samples were also used for RNA-seq analysis as previously reported[21]. The experiments were performed with three biological replicates, and each RNA sample was prepared from a mixture of at least 30 fruits to avoid individual differences among fruits.

For m^{6}A-seq data analysis, the quality of clean reads was assessed using FastQC (version 0.12.0, https://www.bioinformatics.babraham.ac.uk/projects/fastqc/). Sequencing reads were mapped to the *F. vesca* whole genome v4.0.a2 using HISAT2 (version 2.2.1, http://www.ccb.jhu.edu/software/hisat/index.shtml). Peak calling and differential peak analysis were carried out by a R package exomePeak (version 2, https://bioconductor.org/packages/3.9/bioc/html/exomePeak.html) with a criterion of enrichment fold change ≥ 1.5 and P value < 0.05. ANNOVAR (an R package, https://annovar.openbioinformatics.org/en/latest/) was applied to annotate peaks using the strawberry genome annotation file. The de novo and known m^{6}A motifs were identified by HOMER (version 4.1.0, http://homer.ucsd.edu/homer/motif/). The visualization of m^{6}A peaks were performed using Integrated Genome Viewer (IGV, version 2.16.1, http://www.broadinstitute.org/igv/). For RNA-seq analysis, StringTie (version 2.1.2, https://ccb.jhu.edu/software/stringtie/) was employed for calculating fragments per kilobase of exon per million mapped fragments (FPKM). An R package edgeR (https://bioconductor.org/) was used for differential gene expression analysis with a selection criterion of $\log_2(FC) \geq 1$ or $\log_2(FC) \leq -1$ and P value < 0.05.

m^{6}A-IP-qPCR

For m^{6}A-IP-qPCR analysis, mRNAs were fragmented into ~250-nucleotide-long fragments, which were incubated with anti-m^{6}A polyclonal antibody (Synaptic Systems, German, 202003). The immunoprecipitated mRNAs and pre-immunoprecipitated mRNAs (input control) were reverse-transcribed into cDNA and submitted to qPCR analysis using the primers provided in Supplementary Data 16. Relative m^{6}A level in specific region of a transcript was calculated using the $2^{(-\Delta CT)}$ method[62]. The value of the immunoprecipitated sample was normalized against that of the input control[33]. The experiment was performed with three biological replicates.

Transient transformation in strawberry fruit

To construct the RNAi vector, a ~ 300 bp fragment of *FvABF3* or *FvSEP3* coding sequence was cloned and ligated into the pCR8 plasmid, and then restructured into the pK7GWIWGD (II) plasmid. To construct the overexpression vectors, the coding sequence of *FvABF3*, *FvSEP3* or the cDNA fragments of *FvSEP3-WT* and *FvSEP3-Mu896* were separately ligated into the pCAMIA1302 plasmid under the 35S promoter or native promoter. The resulting constructs were separately transformed into *Agrobacterium* strain GV3101, which were subsequently

injected into the fruits of the *Fvalkbh10b* mutant or wild type at the large green stage or the fruits of the *Fvsep3* mutant (kindly provided by Dr. Chunying Kang from Huazhong Agricultural University) at 30 DPA. The empty vectors were used as the negative control. More than 10 fruits were injected for each construct. The infected fruits were remained on the plants to continue growth until the color changes[71]. The primers used for vector construction are listed in Supplementary Data 16.

RNA immunoprecipitation (RIP)

RIP was performed following the method[21] with minor modifications. In brief, the coding region of *FvALKBH10B* was amplified from cDNA of *F. vesca* and inserted into the pCAMBIA1302 vector to generate *35S:FvALKBH10B-HA* construct. The resulting vector and the empty vector control were transformed into the fruits of the *Fvalkbh10b* mutant at large green stage via the *A. tumefaciens*-mediated transformation[66]. After three days of incubation at 23 °C, the fruits with achenes stripped were sliced and fixed in 1% (w/v) formaldehyde. The cross-linked fruits were ground in liquid nitrogen, and then homogenized in lysis buffer containing 50 mM HEPES, pH 7.5, 150 mM KCl, 2 mM EDTA, 0.5% NP-40 (v/v), 0.5 mM DTT, 1× cocktail protease inhibitor (Roche, 4693116001), and 300 units mL^{-1} of RNase Inhibitor (Beyotime, China, R0102-2KU). The mixture was centrifuged at 15,000 × *g* for 20 min after incubation at 4 °C for 1 h. Two hundred microliters of the supernatant were retained as the input control, and the remainder was immunoprecipitated by incubation with HA-Nanoab-Magnetic beads (Lablead, China, HNM-25-1000) at 4 °C for 3 h. The beads were washed five times with lysis buffer, followed by digestion with proteinase K (Takara, Japan, 9034) at 55 °C for 1 h. The immunoprecipitated RNAs and input RNAs were subsequently isolated by Trizol reagent (Invitrogen, USA, 10296028). Equal amounts of RNAs from IP sample and input were reverse-transcribed into cDNA and submitted to qPCR analysis as described above. The primers are provided in Supplementary Data 16.

SELECT analysis

For SELECT analysis, 20 ng of mRNAs were mixed with 40 nM Up-primer, 40 nM Down-primer, and 5 μM dNTP[45]. The mixture was annealed under a temperature gradient of 90 °C for 1 min, 80 °C for 1 min, 70 °C for 1 min, 60 °C for 1 min, 50 °C for 1 min, and 40 °C for 6 min. Subsequently, the mixture was supplemented with 0.01 unit Bst 2.0 DNA polymerase (NEB, USA, M0537S), 0.5 unit SplintR ligase (NEB, USA, M0375S), and 10 nmol ATP to a final volume of 20 μL, and then incubated at 40 °C for 20 min, followed by at 80 °C for 20 min. The mixture was diluted in DEPC-treated water and submitted to RT-qPCR analysis using SELECT-q-F primer and SELECT-q-R primer. Primers used in the SELECT analysis are listed in Supplementary Data 16.

Transcription inhibition and mRNA stability assay

For transcription inhibition assay, 20-d-old seedlings of the wild type or the mutant lines were treated with actinomycin D (Sigma-Aldrich, USA, A4262) at a final concentration of 20 μg mL^{-1}. After 1 h of incubation, 20 seedlings were harvested and considered as time 0 controls, and the subsequent samples were collected every 1 h in triplicate[21]. The mRNA levels were examined by RT-qPCR as described above.

For mRNA stability assay, the intact cDNA fragment of *FvSEP3* containing coding sequence and 3′ UTR was amplified from cDNA of *F. vesca*. The mutated form of the cloned sequence with mutations on the potential m^6A sites were generated using the site-directed mutagenesis kit (Agilent, USA, 200518). The fragments were individually inserted into the pCAMBIA1302 vector, which was subsequently transformed into the fruits of *F. vesca*[71] alone or with the *FvALKBH10B*-expressing vector (pCAMBIA1302-*FvALKBH10B*-HA). After 36 h of incubation, the infection parts of the *F. vesca* were infiltrated with 20 μg mL^{-1} actinomycin D. The fruit discs were taken after 30 min of incubation and considered as time 0 controls. The subsequent samples were taken every 1 h in triplicate[33]. The mRNA levels were then determined by RT-qPCR as described above. All primers are listed in Supplementary Data 16.

Translation efficiency assay

For translation efficiency assay, 5 g of strawberry fruits were ground into fine powder in liquid nitrogen. One gram of sample was applied for total RNA extraction, and the rest was used for polysome extraction[33]. The total RNAs, as well as the polysomal RNAs, were isolated and used for RT-qPCR analysis as described above. Translation efficiency was expressed as the abundance ratio of mRNA in the polysomal RNA versus the total RNA by the cycle threshold (CT) $2^{(-\Delta\Delta CT)}$ method[62] using *ACTIN* (FvH4_6g22300) gene as an internal reference. The primers are listed in Supplementary Data 16.

DAP-seq and data analysis

For DAP-seq, a genomic DNA library of *F. vesca* was constructed by a NEBNext DNA Library Prep Master Mix Set Kit for Illumina (NEB, USA, E7645L). Recombinant FvSEP3 was prepared as a fusion protein with the HaloTag sequence using a TNT SP6 High-Yield Protein Expression System (Promega, USA, L3260). The recombinant FvSEP3-HaloTag protein was purified by Magne HaloTag Beads (Promega, USA, G7281). Then, the FvSEP3-HaloTag Beads mixtures or HaloTag beads were incubated at 4 °C for 2 h with the genomic DNA library. The DNA fragments were eluted from the FvSEP3-HaloTag beads, and then the DAP-seq library was generated using a KAPA Library Quantification Kit (KAPA, USA, KK4824), followed by high-throughput sequencing on a Nova S4 instrument with a paired-end read length of 150-bp (Illumina, USA).

For DAP-seq data analysis, clean reads were mapped to the *F. vesca* whole genome v4.0.a2 annotation using BWA-MEM (https://janis.readthedocs.io/en/latest/tools/bioinformatics/bwa/bwamem.html). Peak identification was performed by MACS2 (version 2.1.1, https://hbctraining.github.io/Intro-to-ChIPseq/lessons/05_peak_calling_macs.html) using default parameters. Only peaks present in both biological replicates were considered as confident peaks. Binding motifs in the peak region were discovered by MEME-ChIP (https://meme-suite.org/meme/doc/meme-chip.html?man_type=web). depTools2 (https://deeptools.readthedocs.io/en/develop/) was used for calculating the distribution frequency of peaks near the transcription start site (TSS) and plotting the distribution of peaks on chromosomes. The binding peaks were visualized by Integrative Genomics Viewer (IGV, version 2.16.1, http://www.broadinstitute.org/igv/). GO enrichment analysis was performed according to the Gene Ontology Resource database (https://geneontology.org/).

Accession numbers

Sequence data from this study can be obtained in the GDR (https://www.rosaceae.org/) database under the following accession numbers: *FvALKBH10B*, FvH4_2g24110; *FvABF3*, FvH4_2g05900; *FvSEP3*, FvH4_4g23530; *FvAREB1*, FvH4_2g34330; *FvDRM3.1*, FvH4_1g24280; *FvCHS1*, FvH4_7g01160; *FvGA3ox1*, FvH4_6g30780; *FvGH3.1*, FvH4_2g04750; *FvNCED1*, FvH4_3g16730; *ACTIN*, FvH4_6g22300.

Statistical analysis

All statistical analyses were conducted with IBM SPSS Statistics (version 20) software. All numerical data are showed as mean ± standard error of mean (SEM) from at least three independent experiments unless otherwise specified in the figure legend and analyzed using unpaired two-sided *t*-test or one-way analysis of variance (ANOVA) with Tukey's HSD test. A *P*-value of <0.05 represents statistically significant. The number of replicates for each experiment is indicated in the figure legends.

Reporting summary

Further information on research design is available in the Nature Portfolio Reporting Summary linked to this article.

Data availability

The m^{6}A-seq and DAP-seq data generated in this study have been separately deposited in the Gene Expression Omnibus database at NCBI under accession codes GSE260825 and GSE260824. The mass spectrometry data generated in this study are provided in the Supplementary Data 17. All other data supporting the findings of this study are available in the main text or the Supplementary Data. Source data are provided with this paper.

References

1. Giovannoni, J. J. Genetic regulation of fruit development and ripening. *Plant Cell* **16**, S170–S180 (2004).
2. Seymour, G. B., Østergaard, L., Chapman, N. H., Knapp, S. & Martin, C. Fruit development and ripening. *Annu. Rev. Plant Biol.* **64**, 219–241 (2013).
3. Huang, W. et al. A molecular framework of ethylene-mediated fruit growth and ripening processes in tomato. *Plant Cell* **34**, 3280–3300 (2022).
4. Jia, H. F. et al. Abscisic acid plays an important role in the regulation of strawberry fruit ripening. *Plant Physiol.* **157**, 188–199 (2011).
5. Chen, T., Qin, G. & Tian, S. Regulatory network of fruit ripening: current understanding and future challenges. *New Phytol.* **228**, 1219–1226 (2020).
6. Kavi Kishor, P. B. et al. Abscisic acid and its role in the modulation of plant growth, development, and yield stability. *Trends Plant Sci.* **27**, 1283–1295 (2022).
7. De Zelicourt, A., Colcombet, J. & Hirt, H. The role of MAPK modules and ABA during abiotic stress signaling. *Trends Plant Sci.* **21**, 677–685 (2016).
8. Chai, Y. M., Jia, H. F., Li, C. L., Dong, Q. H. & Shen, Y. Y. FaPYR1 is involved in strawberry fruit ripening. *J. Exp. Bot.* **62**, 5079–5089 (2011).
9. Boulias, K. & Greer, E. L. Biological roles of adenine methylation in RNA. *Nat. Rev. Genet.* **24**, 143–160 (2023).
10. Tang, J., Chen, S. & Jia, G. Detection, regulation, and functions of RNA N^6-methyladenosine modification in plants. *Plant Commun.* **4**, 100546 (2023).
11. Meyer, K. D. & Jaffrey, S. R. Rethinking m^{6}A readers, writers, and erasers. *Annu. Rev. Cell Dev. Biol.* **33**, 319–342 (2017).
12. Gu, C. et al. RNA m^{6}A modification in cancers: molecular mechanisms and potential clinical applications. *Innovation* **1**, 100066 (2020).
13. Shao, Y., Wong, C. E., Shen, L. & Yu, H. *N*^{6}-methyladenosine modification underlies messenger RNA metabolism and plant development. *Curr. Opin. Plant Biol.* **63**, 102047 (2021).
14. Zheng, G. et al. ALKBH5 is a mammalian RNA demethylase that impacts RNA metabolism and mouse fertility. *Mol. Cell* **49**, 18–29 (2013).
15. Shen, L. Functional interdependence of *N*^{6}-methyladenosine methyltransferase complex subunits in Arabidopsis. *Plant Cell* **35**, 1901–1916 (2023).
16. Luo, S. & Tong, L. Molecular basis for the recognition of methylated adenines in RNA by the eukaryotic YTH domain. *Proc. Natl Acad. Sci. USA* **111**, 13834–13839 (2014).
17. Huang, H. et al. Recognition of RNA *N*^{6}-methyladenosine by IGF2BP proteins enhances mRNA stability and translation. *Nat. Cell Biol.* **20**, 285–295 (2018).
18. Shen, L. S. et al. N^6-methyladenosine RNA modification regulates shoot stem cell fate in *Arabidopsis*. *Dev. Cell* **145**, 186–200 (2016).
19. Scutenaire, J. et al. The YTH domain protein ECT2 is an m^{6}A reader required for normal trichome branching in Arabidopsis. *Plant Cell* **30**, 986–1005 (2018).
20. Zhang, M. et al. Two zinc finger proteins with functions in m^{6}A writing interact with HAKAI. *Nat. Commun.* **13**, 1127 (2022).
21. Duan, H. C. et al. ALKBH10B is an RNA *N*^{6}-methyladenosine demethylase affecting Arabidopsis floral transition. *Plant Cell* **29**, 2995–3011 (2017).
22. Amara, U., Hu, J., Cai, J. & Kang, H. FLK is an mRNA m^{6}A reader that regulates floral transition by modulating the stability and splicing of *FLC* in *Arabidopsis*. *Mol. Plant* **16**, 919–929 (2023).
23. Zhong, S. et al. MTA is an *Arabidopsis* messenger RNA adenosine methylase and interacts with a homolog of a sex-specific splicing factor. *Plant Cell* **20**, 1278–1288 (2008).
24. Zhang, F. et al. The subunit of RNA N6-methyladenosine methyltransferase OsFIP regulates early degeneration of microspores in rice. *PLoS Genet.* **15**, e1008120 (2019).
25. Wang, C. et al. FIONA1 is an RNA *N*^{6}-methyladenosine methyltransferase affecting Arabidopsis photomorphogenesis and flowering. *Genome Biol.* **23**, 40 (2022).
26. Jiang, B. et al. Light-induced LLPS of the CRY2/SPA1/FIO1 complex regulating mRNA methylation and chlorophyll homeostasis in *Arabidopsis*. *Nat. Plants* **9**, 2042–2058 (2023).
27. Fustin, J. M. et al. Two Ck1δ transcripts regulated by m^{6}A methylation code for two antagonistic kinases in the control of the circadian clock. *Proc. Natl Acad. Sci. USA* **115**, 5980–5985 (2018).
28. Wang, X. et al. A photoregulatory mechanism of the circadian clock in *Arabidopsis*. *Nat. Plants* **7**, 1397–1408 (2021).
29. Zhang, K. et al. The dynamics of *N*^{6}-methyladenine RNA modification in interactions between rice and plant viruses. *Genome Biol.* **22**, 189 (2021).
30. Fan, W. et al. m^{6}A RNA demethylase AtALKBH9B promotes mobilization of a heat-activated long terminal repeat retrotransposon in *Arabidopsis*. *Sci. Adv.* **9**, eadf3292 (2023).
31. Lee, K. P. et al. The m^{6}A reader ECT1 drives mRNA sequestration to dampen salicylic acid-dependent stress responses in Arabidopsis. *Plant Cell* **36**, 746–763 (2024).
32. Prall, W. et al. Pathogen-induced m^{6}A dynamics affect plant immunity. *Plant Cell* **35**, 4155–4172 (2023).
33. Zhou, L. et al. N^6-methyladenosine RNA modification regulates strawberry fruit ripening in an ABA-dependent manner. *Genome Biol.* **22**, 168 (2021).
34. Zhou, L., Tian, S. & Qin, G. RNA methylomes reveal the m^{6}A-mediated regulation of DNA demethylase gene *SlDML2* in tomato fruit ripening. *Genome Biol.* **20**, 156 (2019).
35. Mielecki, D. et al. Novel AlkB dioxygenases–alternative models for in silico and in vivo studies. *PLoS ONE* **7**, e30588 (2012).
36. Gutzat, R. et al. *Arabidopsis* shoot stem cells display dynamic transcription and DNA methylation patterns. *EMBO J.* **39**, e103667 (2020).
37. Liao, X. et al. Interlinked regulatory loops of ABA catabolism and biosynthesis coordinate fruit growth and ripening in woodland strawberry. *Proc. Natl Acad. Sci. USA* **115**, E11542–E11550 (2018).
38. Hengwei, Y. et al. Research progress of m^{6}A regulation during animal growth and development. *Mol. Cell. Probes* **65**, 101851 (2022).
39. Zhou, L. et al. m^{6}A-mediated regulation of crop development and stress responses. *Plant Biotechnol. J.* **20**, 1447–1455 (2022).
40. Wang, X. et al. *N*^{6}-methyladenosine-dependent regulation of messenger RNA stability. *Nature* **505**, 117–120 (2014).
41. Wei, L. H. et al. The m^{6}A reader ECT2 controls trichome morphology by affecting mRNA stability in Arabidopsis. *Plant Cell* **30**, 968–985 (2018).

42. Pi, M. et al. The MADS-box gene *FveSEP3* plays essential roles in flower organogenesis and fruit development in woodland strawberry. *Hortic. Res.* **8**, 247 (2021).
43. Furihata, T. et al. Abscisic acid-dependent multisite phosphorylation regulates the activity of a transcription activator AREB1. *Proc. Natl Acad. Sci. USA* **103**, 1988–1993 (2006).
44. Cheng, J. et al. Downregulation of RdDM during strawberry fruit ripening. *Genome Biol.* **19**, 212 (2018).
45. Xiao, Y. et al. An elongation- and ligation-based qPCR amplification method for the radiolabeling-free detection of locus-specific N^6-methyladenosine modification. *Angew. Chem. Int. Ed. Engl.* **57**, 15995–16000 (2018).
46. O'Malley, R. C. et al. Cistrome and epicistrome features shape the regulatory DNA landscape. *Cell* **165**, 1280–1292 (2016).
47. Ito, Y. et al. DNA-binding specificity, transcriptional activation potential, and the rin mutation effect for the tomato fruit-ripening regulator RIN. *Plant J.* **55**, 212–223 (2008).
48. Staswick, P. E. et al. Characterization of an Arabidopsis enzyme family that conjugates amino acids to indole-3-acetic acid. *Plant Cell* **17**, 616–627 (2005).
49. Sun, T. P. The molecular mechanism and evolution of the GA-GID1-DELLA signaling module in plants. *Curr. Biol.* **21**, R338–R345 (2011).
50. Castillejo, C. et al. Allelic variation of *MYB10* is the major force controlling natural variation in skin and flesh color in strawberry (*Fragaria spp.*) fruit. *Plant Cell* **32**, 3723–3749 (2020).
51. Jia, G. et al. N^6-methyladenosine in nuclear RNA is a major substrate of the obesity-associated FTO. *Nat. Chem. Biol.* **7**, 885–887 (2011).
52. Martínez-Pérez, M. et al. *Arabidopsis* m^6A demethylase activity modulates viral infection of a plant virus and the m^6A abundance in its genomic RNAs. *Proc. Natl Acad. Sci. USA* **114**, 10755–10760 (2017).
53. Li, F. et al. N^6-methyladenosine modulates nonsense-mediated mRNA decay in human glioblastoma. *Cancer Res.* **79**, 5785–5798 (2019).
54. Zhang, S. et al. m^6A demethylase ALKBH5 maintains tumorigenicity of glioblastoma stem-like cells by sustaining FOXM1 expression and cell proliferation program. *Cancer Cell* **31**, 591–606.e6 (2017).
55. Du, Y. et al. SUMOylation of the m^6A-RNA methyltransferase METTL3 modulates its function. *Nucleic Acids Res.* **46**, 5195–5208 (2018).
56. Sun, H. L. et al. Stabilization of ERK-phosphorylated METTL3 by USP5 increases m^6A methylation. *Mol. Cell* **80**, 633–647.e7 (2020).
57. Sun, L. et al. Lactylation of METTL16 promotes cuproptosis via m^6A-modification on *FDX1* mRNA in gastric cancer. *Nat. Commun.* **14**, 6523 (2023).
58. Lv, D. et al. EGFR promotes ALKBH5 nuclear retention to attenuate N6-methyladenosine and protect against ferroptosis in glioblastoma. *Mol. Cell* **83**, 4334–4351.e4337 (2023).
59. Fujii, H. et al. In vitro reconstitution of an abscisic acid signalling pathway. *Nature* **462**, 660–664 (2009).
60. Hwang, K., Susila, H., Nasim, Z., Jung, J. Y. & Ahn, J. H. *Arabidopsis* ABF3 and ABF4 transcription factors act with the NF-YC complex to regulate *SOC1* expression and mediate drought-accelerated flowering. *Mol. Plant* **12**, 489–505 (2019).
61. Chen, K. et al. Abscisic acid dynamics, signaling, and functions in plants. *J. Integr. Plant Biol.* **62**, 25–54 (2020).
62. Schmittgen, T. D. & Livak, K. J. Analyzing real-time PCR data by the comparative C_T method. *Nat. Protoc.* **3**, 1101–1108 (2008).
63. Sparkes, I. A., Runions, J., Kearns, A. & Hawes, C. Rapid, transient expression of fluorescent fusion proteins in tobacco plants and generation of stably transformed plants. *Nat. Protoc.* **1**, 2019–2025 (2006).
64. Lei, R., Qiao, W., Hu, F., Jiang, H. & Zhu, S. A simple and effective method to encapsulate tobacco mesophyll protoplasts to maintain cell viability. *MethodsX* **2**, 24–32 (2014).
65. Jia, H. et al. Abscisic acid and sucrose regulate tomato and strawberry fruit ripening through the abscisic acid-stress-ripening transcription factor. *Plant Biotechnol. J.* **14**, 2045–2065 (2016).
66. Li, X. et al. Deciphering the regulatory network of the NAC transcription factor FvRIF, a key regulator of strawberry (*Fragaria vesca*) fruit ripening. *Plant Cell* **35**, 4020–4045 (2023).
67. Ji, D., Cui, X., Qin, G., Chen, T. & Tian, S. SlFERL interacts with S-adenosylmethionine synthetase to regulate fruit ripening. *Plant Physiol.* **184**, 2168–2181 (2020).
68. Ma, X. et al. A robust CRISPR/Cas9 system for convenient, high-efficiency multiplex genome editing in monocot and dicot plants. *Mol. Plant* **8**, 1274–1284 (2015).
69. Oosumi, T. et al. High-efficiency transformation of the diploid strawberry (*Fragaria vesca*) for functional genomics. *Planta* **223**, 1219–1230 (2006).
70. Dominissini, D., Moshitch-Moshkovitz, S., Salmon-Divon, M., Amariglio, N. & Rechavi, G. Transcriptome-wide mapping of N^6-methyladenosine by m^6A-seq based on immunocapturing and massively parallel sequencing. *Nat. Protoc.* **8**, 176–189 (2013).
71. Hoffmann, T., Kalinowski, G. & Schwab, W. RNAi-induced silencing of gene expression in strawberry fruit (*Fragaria* × *ananassa*) by agroinfiltration: a rapid assay for gene function analysis. *Plant J.* **48**, 818–826 (2006).

Acknowledgements

We would like to thank Hang Su (Institute of Botany, Chinese Academy of Sciences) for analysis of LC-MS/MS and Jingquan Li (Institute of Botany, Chinese Academy of Sciences) for assistance with confocal microscopy. We thank Yaoguang Liu (South China Agriculture University) for providing the pYLCRISPR/Cas9Pubi-H binary vector and Chunying Kang (Huazhong Agricultural University) for providing the *Fvsep3* mutant. We also thank Yongji Biotechnology Co. Ltd. (Guangzhou, China) for DAP-seq data analysis and LC-Bio Technology CO., Ltd for assistance with m^6A-seq assay. This work was supported by the National Natural Science Foundation of China (No. 31925035 to G.Q.), the CAS Project for Young Scientists in Basic Research (YSRB-093 to G.Q.), and the Shandong Provincial Key Research and Development Program (2022TZXD0023 to G.Q.).

Author contributions

G.Q. designed the research. R.T., X.D., L.Z., G.G., J.L., Y.W., and X.S. performed the experiments. G.Q. and R.T. analyzed the data. G.Q. and R.T. wrote the manuscript.

Competing interests

The authors declare no competing interests.

Additional information

Supplementary information The online version contains supplementary material available at https://doi.org/10.1038/s41467-024-55294-8.

Correspondence and requests for materials should be addressed to Guozheng Qin.

Peer review information *Nature Communications* thanks Hunseung Kang, Zhongchi Liu and the other, anonymous, reviewer for their contribution to the peer review of this work. A peer review file is available.